



# Kinematic Motion Planning for a 7-Axis Robotic Arm (LWA70 by Schunk)

**Written by:**

***Shehab Mohammed***

VT 2016

Kinematic Motion Planning for a 7-Axis Robotic Arm (LWA70 by Schunk).  
Master Thesis in Electronic Engineering (Specialization Robotics and Control), 5EL205, 30 hp.



**Supervised by:**  
**Leonid Freidovich**  
**Associate Professor, Umeå University**

**Assessed by:**  
**Sven Rönnbäck**  
**Associate Professor, Umeå University**

**Defended:**  
**November 9 2016 At Umeå University**

**Opponent:**  
**Hongzhe Lee**

## Abstract

Redundant manipulators are widely used because they have a greater dexterity and versatility than nonredundant manipulators. In the redundant manipulators, the number of degrees of freedom are more than the required to manipulate objects at the task space, which leads to a possibility to generate infinite number of solutions. For this reasons it has been a hot research topic to exploit the redundancy. This thesis work is focus on modeling and controlling redundant robot manipulator with seven degree of freedom (LWA 10 kg payload by Schunk). A literature review has been prepared on the existing methods of exploiting the redundancy in the 7-DOF manipulators at the velocity and position levels. The forward kinematic equations are derived using the Denavit-Hartenberg method. The inverse kinematic problem is solved and the redundancy is exploited at the position level to avoid the computational complexity and inaccuracy associated with exploiting the redundancy at the velocity level. The joint angles of the manipulator are computed in term of a redundancy parameter defining the self-motion in the manipulator. The relation between the joint angles and the redundancy parameter is exploited to avoid selecting the arm angles that violate the joint limits. The singularity configurations and robot workspace are also studied in this thesis. An example is presented on how the self-motion of the arm appears when the end-effector is stationary. The methods are applied to follow straight line trajectories while preventing the joints to exceed the limits. The results found showed how exploiting the redundancy at the position level is being exact with low computational cost. The validity of the methods is verified by Robotics Toolbox simulations.

## Acknowledgments

I would like to thank my supervisor Leonid Freidovich. He has been continuously supporting me academically and holding me up in a difficult time that I went through because of the war in my home country.

I would like also to give special thank for the Swedish Institute (SI) for funding me though out my master studies. Coming to Sweden to pursue master's program in robotics and control would not have been possible for me without the opportunity I offered by the Swedish Institute.

I would like to express my gratitude to Sven Rönnbäck for his advices thought out my master studies.

Lastly, I'm very grateful to my family and friends for their support and love.



November 9, 2016

Umeå, Sweden

# Contents

<b>1</b>	<b>Introduction</b>	<b>9</b>
1.1	Background . . . . .	9
1.2	Motivation . . . . .	9
1.3	Objectives . . . . .	10
1.4	Robot Model . . . . .	11
1.5	Project requirements . . . . .	12
1.6	Resources . . . . .	12
1.7	Research outline . . . . .	13
<b>2</b>	<b>Literature Review</b>	<b>15</b>
2.1	Redundancy resolution at velocity level . . . . .	16
2.2	Redundancy resolution at position level . . . . .	18
2.3	Conclusions . . . . .	19
<b>3</b>	<b>Forward Kinematics</b>	<b>21</b>
3.1	Denavit-Hartenberg representation . . . . .	22
3.2	Assigning the coordinate frames . . . . .	25
3.3	Forward kinematics equations . . . . .	26
<b>4</b>	<b>Inverse Kinematics and Redundancy Resolution</b>	<b>31</b>
4.1	Redundancy parameterization . . . . .	32
4.2	Joint angles computations . . . . .	36
4.2.1	Elbow joint angle ( $\theta_4$ ) . . . . .	36

4.2.2	Shoulder joint angles ( $\theta_1$ , $\theta_2$ and $\theta_3$ ) . . . . .	37
4.2.3	Wrist joint angles ( $\theta_5$ , $\theta_6$ and $\theta_7$ ) . . . . .	42
4.3	The effect of the arm angle on the joint angles . . . . .	45
4.4	Redundancy resolution for joint limits . . . . .	52
4.4.1	Joint angles without critical arm angles . . . . .	53
4.4.2	Joint angles with critical arm angles (Cyclic type) . . . . .	55
4.5	Singularity configurations and avoidance . . . . .	60
4.5.1	Kinematic singularities . . . . .	60
4.5.2	Algorithmic Singularities . . . . .	62
<b>5</b>	<b>Results and Analysis</b>	<b>63</b>
5.1	Algorithm summary . . . . .	64
5.2	Robot workspace . . . . .	67
5.3	The redundancy circle at a stationary end-effector . . . . .	69
5.4	Redundancy resolution under joint limits . . . . .	72
5.5	Straight line Cartesian trajectories . . . . .	78
<b>6</b>	<b>Discussion and Conclusions</b>	<b>89</b>
6.1	Discussion . . . . .	89
6.2	Conclusions . . . . .	92
6.3	Future work . . . . .	93
6.4	Ethical aspects . . . . .	93

# List of Tables

1.1	Project requirements . . . . .	12
1.2	Human resources . . . . .	12
1.3	Computer resources . . . . .	13
3.1	Denavit-Hartenberg parameters . . . . .	26
4.1	$\psi_c$ is minimum . . . . .	51
4.2	$\psi_c$ is maximum . . . . .	51
5.1	The lower and upper limits of each joint . . . . .	67
5.2	Assumed stricter upper and lower limits . . . . .	73



# List of Figures

1-1	Dexterous lightweight arm 7-DOF (SCHUNK)	11
3-1	The manipulator structure	22
3-2	The coordinate frames assigned to the manipulator	25
4-1	Arm angle definition	33
4-2	Joint angle 4 calculation	36
4-3	The reference joint angles calculation	37
4-4	Example profile of the joint angles $\theta_1$ , $\theta_3$ , $\theta_5$ or $\theta_7$ with respect to the redundancy parameter when (4.53) is satisfied	47
4-5	Example profile of the joint angles $\theta_1$ , $\theta_3$ , $\theta_5$ or $\theta_7$ with respect to the redundancy parameter when (4.55) is satisfied	49
4-6	Example profile of the joint angles $\theta_2$ or $\theta_6$ with respect to the redundancy parameter where $\theta \neq 0^\circ$ and $\theta \neq 180^\circ$	51
4-7	The feasible arm angle of the joint angles $\theta_1$ , $\theta_3$ , $\theta_5$ or $\theta_7$ when (4.55) is satisfied	54
4-8	Case 1: The full range of the arm angle is acceptable	55
4-9	Excluding the arm angle range when the maximum joint angle is greater than the upper limit	56
4-10	Excluding the arm angle range when the minimum joint angle is less than the lower limit	57
4-11	Two arm angle domains to be eliminated	58
4-12	The entire domain of the arm angle is not acceptable:(a) when $\theta_{max} < \theta_L$ (b): $\theta_{min} > \theta_U$	59

4-13	Elbow singularity configuration. . . . .	61
4-14	Shoulder singularity configuration. . . . .	61
5-1	The robot workspace. . . . .	68
5-2	The joints curves with respect to the arm angle at pose in (5.2). . . . .	70
5-3	Redundancy circle at the pose in (5.2). . . . .	71
5-4	Forward and inverse kinematics block diagram. . . . .	72
5-5	Joint angles versus the arm angle at pose in (5.3). . . . .	73
5-6	Straight line trajectory along X-axis. . . . .	78
5-7	Simulation results of tracking straight line along X-axis when arm angle is as in (5.4) where (a): The elbow movement (b): The seven joint angle trajectories. . . . .	80
5-8	Simulation results of tracking straight line along X-axis when arm angle is as in (5.5) where (a): The elbow movement (b): The seven joint angle trajectories. . . . .	81
5-9	Straight line trajectory along Y-axis. . . . .	82
5-10	Simulation results of tracking straight line along Y-axis when arm angle is as in (5.4) where (a): The elbow movement (b): The seven joint angle trajectories. . . . .	83
5-11	Simulation results of tracking straight line along Y-axis when arm angle is as in (5.5) where (a): The elbow movement (b): The seven joint angle trajectories. . . . .	84
5-12	Straight line trajectory along Z-axis. . . . .	85
5-13	Simulation results of tracking straight line along Z-axis when arm angle is maximum where (a): The elbow movement (b): The seven joint angle trajectories. . . . .	86
5-14	Simulation results of tracking straight line along Z-axis when arm angle is as in (5.4) where (a): The elbow movement (b): The seven joint angle trajectories. . . . .	87

# **Chapter 1**

## **Introduction**

### **1.1 Background**

Humans are made of muscles, bones and senses. We sense the surroundings by touch and vision as a measure to use the muscles for controlling ourselves. Robots are built from links, actuators and joints in various configurations, and are equipped with sensors. Robot kinematics study configurations of multi-degree of freedom kinematic chains that form the structure of robotic systems [1].

To accomplish a desired task by end-effectors of robot manipulators, we need to study the robots kinematics structure and motion planning. Kinematics can be categorized as forward kinematics and inverse kinematics. This thesis work will be on a 7-DOF Articulated Robot manipulator (LWA 10 kg payload) by SCHUNK. This dexterous robot has 7 degrees of freedom (revolute joints), and it is a redundant manipulator. The current chapter presents a motivation on the redundant manipulators, the objectives of the project, overview of the robot model and the project requirements

### **1.2 Motivation**

In working environments of robot manipulators, there are needs for performing secondary tasks such as avoiding collisions with obstacles, avoiding the joints limits,

minimizing the energy consumption and execution time, increasing the manipulability, and maximizing the reachable region by the end-effector in the robot workspace. The needs for performing these additional tasks while the primary task, such as following trajectory performed by the end-effector, is not affected, led to introducing the redundant manipulators, which have a greater dexterity and versatility than the nonredundant manipulators. Redundancy in the robot manipulators means that the number of the joint space variables are greater than the number of the task space variables. Manipulators with greater than 6 axes are called redundant manipulators because six axes is the number of joints required to reach an arbitrary position and orientation of the end-effector within its working space [2][3][4][5]. The 7-axes can be used for additional tasks for these reasons, several researchers have been devoting efforts toward this kind of arms.

### **1.3 Objectives**

The main objectives expected to meet in this thesis work are as follows:

1. Preparing a literature survey on the solutions of the inverse kinematics for 7-DOF articulated robot manipulator with emphasis on exploiting the kinematic redundancy.
2. Developing and testing MATLAB/SIMULINK software blocks implementing the forward kinematics.
3. Solving the inverse kinematics problem with an intelligent use of the redundancy. The results to be implemented in MATLAB/SIMULINK.
4. Developing a demonstration scenario possibly by moving the end-point along straight lines (vertical:up and down and horizontal: left and right, forward and backward).

## 1.4 Robot Model

The light weight arm (10kg payload) by SCHUNK has seven revolute joints. The arm has Spherical-Revolution-Spherical (SRS) manipulator structure. The first three joints can be combined as a virtual spherical joint because their axes intersect at a single point, same apply to the last three joints. There is a revolution joint between these two virtual spherical joints. The structure of the arm make it similar to a human arm to form shoulder joints (1,2 and 3)-elbow joint(4)-wrist joints (5,6 and 7). This kind of manipulators are also called anthropomorphic arms [4] [6][7]. Figure 1.1 shows the robot model with a sketch identifying the joint angles. The arm virtual model was downloaded from [8] as STL format files partitions and assembled using SolidWork software. The technical data implemented in this work are the (LWA) arm data available at the Department of Applied Physics and Electronics, Umeå University. More details about the arm structure will be presented in chapters 3 and 4.

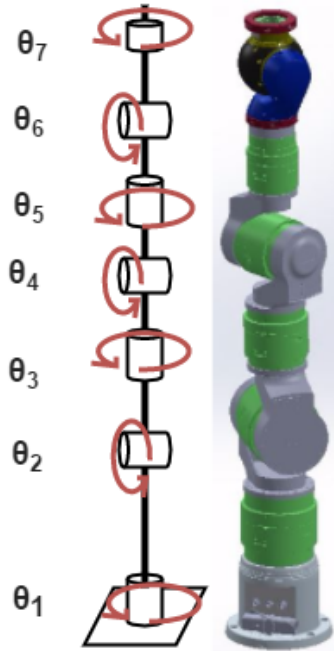


Figure 1-1: Dexterous lightweight arm 7-DOF (SCHUNK).

## 1.5 Project requirements

This thesis work is conducted as a master thesis project at the Department of Applied Physics and Electronics at Umeå University. Certain requirements, resources and deliveries are required for the project. Table 1.1 presents the thesis requirements list.

Table 1.1: Project requirements

No	Activity	Description
1	Project formulation	Discussion and approval of the project with supervisor.
2	Preliminary Study	Brief literature survey on the previous related articles and discussion on (objectives, resources, requirements list).
3	Literature survey	Comprehensive literature survey on inverse kinematics for redundant manipulators.
4	Forward kinematics	Modelling and deriving the forward kinematics equations of the manipulator.
5	Inverse kinematics	Deriving the inverse kinematics algorithms of the manipulator exploiting the redundancy.
6	Results Tests	Presenting scenario to test the forward and inverse kinematics algorithms.
7	Results Analysis	Discussing the obtained results

## 1.6 Resources

The project resources are limited to individuals and computer software. Table 1.3 lists the human resources and responsibilities for each one. Computer software resources are presented in table 1.4.

Table 1.2: Human resources

Human resources	Role	Responsibility
Dr. Leonid Freidovich	Supervisor	Evaluation, giving advices and suggestions on the conducted work.
Dr. Sven Rönnbäck	Thesis Examiner	Grading the thesis work.
Shehab Moahmmed	Student	Achieving the project objectives.

Table 1.3: Computer resources

Computer resources	Propose	Provided by
Matlab/Simulink	To implement and simulate the obtained results	Umeå University (Math-work Student License).
Latex	Report documentation	Open source.

## 1.7 Research outline

The structure of this thesis work is the following. The next chapter 2 gives a literature survey on the inverse kinematics of redundant manipulators by reviewing the related articles. Chapter 3 presents the forward kinematics methods of the 7-DOF articulated robot manipulator model (LWA 10kg payload) by SCHUNK . Chapter 4 contains the inverse kinematics methods and the algorithms of exploiting the redundancy. In chapter 5 computer simulation results are presented and chapter 6 discusses the overall performance of the implemented algorithms, topics for future, work ethics and conclusions.



# Chapter 2

## Literature Review

For decades, a great amount of work has been dedicated by researchers on kinematics modelling and control design for redundant manipulators. This chapter presents an overview of the methods used by researchers to solve the inverse kinematics problems of redundant manipulators and to exploit the redundancy. Forward kinematics is a straightforward problem. Therefore, the existing methods in the literature can be used to solve this problem. Denavit-Hartenberg method is used in this thesis work to derive the forward kinematics. Conversely, Inverse kinematics problems are tricky and indirect to solve. The existing literature on solving the inverse kinematics problems do not provide a general solution.

Redundant manipulators have an infinite number of configurations that lead to the same end-effector desired position and orientation. A number of solution techniques for solving the inverse kinematic problem for redundant manipulators have been proposed by researchers. Most of these suggested methods are established with intelligent use of redundancy based on a given additional task requirement such as avoiding joint limits, avoiding singularities, manipulability enhancement, collision avoidance and reconfiguring the structure of the arm to find better postures of the manipulator without changing the end-effector position and orientation (self-motion) [7] [9][10][11]. Some researchers directed their efforts to solve the inverse problem of redundant manipulators by iterative (numerical) methods solving the problem at the velocity level. Other published papers are discussing the inverse problems of redun-

dant manipulators in analytical (algebraic) methods by solving the problem of inverse kinematics at the position level.

Each of these proposed methods has some cons and pros. For example, solving the inverse kinematics problem by analytical methods usually gives exact solutions unlike numerical methods and it is faster than the other methods [12]. However, these methods become more complicated to apply in manipulators with high number of axes [4] [9].

## 2.1 Redundancy resolution at velocity level

Iterative methods solve the inverse kinematics problems by approximating the solution and updating it until convergence, which is achieved by minimizing the difference between the current and desired positions [13]. This method generates a continues solution and usually can be used for tracking a trajectory. However, it is computationally expensive, it is not totally free from avoiding singularities and it is difficult to exactly evaluate the reachable region of the manipulator tool in the global configuration space under the constraints of joint limits [4][14].

To the best of my knowledge, Whitney [15] was the first who proposed a method to solve the inverse kinematics of redundant manipulator at the velocity level using Jacobian Moore-Penrose pseudoinverse matrix. This method is a local optimization technique that generates from infinite solutions the minimum norm joint velocities instantaneously. However, this method does not provide a global velocity minimization of the whole arm because Jacobian matrix is not feasible at and in the neighborhood of the singular points, which means that the kinematic singularity avoidance is not guaranteed [10] [16].

The pseudo-inverse method provides solutions for the primary tasks only such as following a desired workspace trajectory. The redundancy of the manipulator in this method can not be exploited for any extra tasks such as obstacle avoidance, singularity avoidance and so on. For this reason, improvements to this method were proposed. One solution is adding a null space term (control term) to the pseudo-inverse Jacobian-based in order to exploit redundancy to perform secondary tasks that do not affect the primary tasks [17][18]. Another method proposed for exploiting the redundancy to perform a secondary defined task is the augmented (extended) Jacobian method [19]. This method is easier computationally since it uses matrix inversion because in this method the extended Jacobain matrix is always square. However, the problem with this method is that the secondary task must exist at all times, this can not happen for obstacle avoidance or keeping away from joint limits, which do not exist at all times [20].

The shortcoming of singularity robustness in Jacobian based method was discussed by [21]. Wampler proposed the Damped Least-Squares methods for singularity robustness, to tackle the failure of the Jacobian matrix near kinematic singularities. The problem with this method is the selection of the damping factor because selecting a small value gives an accurate solution but low singularity robustness and choosing a high value of damping factor gives high robustness but it reduces the accuracy of the solution [16].

The matter of choosing the damping factor was discussed by [22]. Nakamura and Hanafusa suggested a method for varying the damping factor based on measuring the distance from the singularity at the current configuration of the manipulator. [23] suggested that the smallest singular value in the Jacobian matrix can be used as an effective measure of the distance from the singular configuration. Some researchers focused on resolving the redundancy at the velocity level using closed-loop inverse kinematics (CLIK) algorithm such as [24].

## 2.2 Redundancy resolution at position level

On the other hand some researchers efforts have been devoted to finding an analytical solution exploiting redundancy using position-based kinematic control methods to avoid the numerical instability and computational complexity associated with velocity-based kinematic control. One of the most recently published papers is [4], which proposed a methodology to analytically compute all the feasible inverse solutions of a 7-DOF humanoid like redundant manipulators in the position domain constrained by joint limits. The method proposed in this article used the arm angle parameterization methods proposed by [7] for redundancy resolution. The arm angle parameterization method states that the self-motion of the manipulator can be represented by the arm angle. The arm angle is defined as the angle between a reference plane and the arm plane, which is spanned by the shoulder, elbow and wrist. In [7] the reference plane can be determined by a fixed vector. However, if this arbitrary chosen fixed vector and the axis connecting the shoulder and wrist are collinear, the reference plane is indeterminate. For this reason, [4] defined alternative definition for the reference plane by fixing joint angle 3 in the manipulator to zero and considering the plane spanned by the shoulder, elbow and wrist as the reference plane.

The arm angle parameterization was also used in [11], the configuration control proposed in this method was to perform elbow control and obstacle avoidance. However, no description was presented on how to avoid the joint limits. Improvement to this method was addressed in [25] to avoid singularities and allow the user to assign appropriate priorities to the task requirements.

Lee and Bejczy [14] presented a new method of kinematic control based on joint parameterization of redundant manipulators at the position level. The method analyzing the geometric features and mechanical structure of the arm and form a closed form of parameterized inverse kinematic solution. Although this method may be used for different kinds of arms, the parameterization of redundant joints may become hard for some kinds of manipulators. There was no joint limit constrains imposed in the

method. Another proposed method [26] was implemented in real time on a humanoid robot using analytical method. The results obtained are accurate and have low computation cost. However, this method can not be applied to humanoid robots with higher degree of redundancy.

### 2.3 Conclusions

My conclusion is that in the early stage of the research in this domain there was more concern on the iterative methods, recently analytical methods of redundant manipulator take more interest among the researchers in this area. There is also a trade-off among the proposed methods between the solution accuracy and computational complexity.



# Chapter 3

## Forward Kinematics

This chapter discusses and develops the forward kinematics equations of the considered 7-DOF articulated robot manipulator (LWA 10 kg payload). The forward kinematics determine the position and orientation of the end-effector when the joint angles values are given by mapping the joint space to the task space. The manipulator considered in this project has seven revolute joints rotating around fixed axis on previous links. As mentioned before, the 7-DOF manipulator has a similar structure with human arm. The arm has 7 revolute joints arranged to form the shoulder, elbow, and wrist portions as shown in Figure 3-1. Forward kinematics problem has no complexity to derive the equations comparing to the inverse kinematics because it is a straightforward problem. Hence, there is always a forward kinematics solution of a manipulator. Denavit-Hartenberg method is the most common method for describing the manipulator kinematics that led to derive the forward kinematics equations.

This chapter is organized in the following manner. The first section discusses the Denavit-Hartenberg convention method, the second section presents the procedures of assigning the coordinate frames based on Denavit-Hartenberg conditions and the last section shows the derived forward kinematics equations for the manipulator.

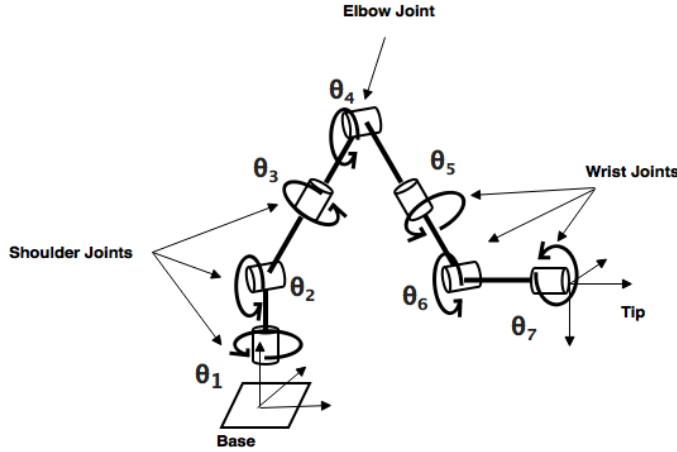


Figure 3-1: The manipulator structure.

### 3.1 Denavit-Hartenberg representation

The forward kinematics of the arm can be developed by a systemic procedure using a combination of conventions to determine and analyze the successive effect of the consecutive joint motions to finally place the end-effector at a specific position and orientation. These conversions simplifying the intricacy of the forward kinematics analysis in the complex arm with higher number of axes. Solving the forward kinematics problem can be accomplished by calculating the transformation between the fixed base frame and the end-effector frame. The Denavit-Hartenberg procedure is the ordinarily convention used to calculate the transformation between the frame [27]. Each joint in the manipulator connects two links where every joint  $i$  connects the link  $i-1$  to the link  $i$ . When joint  $i$  is actuated the link  $i$  moves. The link 0 is always fixed. The notations used in this work is similar to the notations in the standard robotics books such as [16] [28].

In Denavit-Hartenberg method, the homogeneous transformation matrix is represented by a product of four basic transformations. These transformations are two translations and two rotations parametrized by the four Denavit-Hartenberg parameters as (3.1) equation illustrates.

$$\begin{aligned}
{}^{i-1}T_i &= Rot_{z_i}(\theta_i)Trans_{z_i}(d_i)Trans_{x_i}(a_i)Rot_{x_i}(\alpha_i) \\
&= \begin{bmatrix} \cos(\theta_i) & -\sin(\theta_i) & 0 & 0 \\ \sin(\theta_i) & \cos(\theta_i) & 0 & 0 \\ 0 & 0 & 1 & 0 \\ 0 & 0 & 0 & 1 \end{bmatrix} \begin{bmatrix} 1 & 0 & 0 & 0 \\ 0 & 1 & 0 & 0 \\ 0 & 0 & 1 & d_i \\ 0 & 0 & 0 & 1 \end{bmatrix} \begin{bmatrix} 1 & 0 & 0 & a_i \\ 0 & 1 & 0 & 0 \\ 0 & 0 & 1 & 0 \\ 0 & 0 & 0 & 1 \end{bmatrix} \begin{bmatrix} 1 & 0 & 0 & 0 \\ 0 & \cos(\alpha_i) & -\sin(\alpha_i) & 0 \\ 0 & \sin(\alpha_i) & \cos(\alpha_i) & 0 \\ 0 & 0 & 0 & 1 \end{bmatrix} \\
&= \begin{bmatrix} \cos(\theta_i) & -\sin(\theta_i)\cos(\alpha_i) & \sin(\theta_i)\sin(\alpha_i) & a_i\cos(\theta_i) \\ \sin(\theta_i) & \cos(\theta_i)\cos(\alpha_i) & -\cos(\theta_i)\sin(\alpha_i) & a_i\sin(\theta_i) \\ 0 & \sin(\alpha_i) & \cos(\alpha_i) & d_i \\ 0 & 0 & 0 & 1 \end{bmatrix} \tag{3.1}
\end{aligned}$$

where  $\theta_i$  is the joint angle,  $d_i$  is the link offset,  $a_i$  is the link length and  $\alpha_i$  is the link twist.

The matrix  ${}^{i-1}T_i$  is a function of a single variable  $\theta_i$  because the manipulator in this study has only revolute joints, the remain three parameters are constant for each link. The joint angle  $\theta_i$  is the angle measured about  $z_{i-1}$  between  $x_{i-1}$  and  $x_i$ . The link offset  $d_i$  is the distance from  $o_{i-1}$  to the intersection of the  $x_i$  and  $z_{i-1}$  axes along  $z_{i-1}$ . The link length  $a_i$  is the distance from  $o_i$  to the intersection of the  $x_i$  and  $z_{i-1}$  axes along  $x_i$ . The link twist  $\alpha_i$  is the angle measured about  $x_i$  between  $z_{i-1}$  and  $z_i$ . The homogeneous transformation matrix  ${}^{i-1}T_i$  expresses the position of joint frame center  $o_i$  and orientation of the attached frame  $i$  with respect to the previous joint frame  $i-1$ . So the transformation from the base to the end-effector is given by (3.2)

$${}^0T_7 = {}^0T_1{}^1T_2{}^2T_3{}^3T_4{}^4T_5{}^5T_6{}^6T_7 \tag{3.2}$$

Where the transformation matrix  ${}^{i-1}T_i$  is given by the rotation matrix  ${}^{i-1}R_i$  and the translation vector  ${}^{i-1}p_i$  as shown in equation(3.3).

$${}^{i-1}T_i = \begin{bmatrix} {}^{i-1}R_i & {}^{i-1}p_i \\ 0 & 1 \end{bmatrix} \tag{3.3}$$

The rotation matrix  ${}^{i-1}R_i$  in Denavit-Hartenberg method can be combination of rotations around z and x. The corresponding rotation matrices are shown in equation (3.4).  ${}^{i-1}p_i$  is a 3 by 1 vector that represents coordinates of the position of the frame center ( $p_x, p_y$  and  $p_z$ ).

$$R_z = \begin{bmatrix} \cos(\theta_i) & -\sin(\theta_i) & 0 \\ \sin(\theta_i) & \cos(\theta_i) & 0 \\ 0 & 0 & 1 \end{bmatrix}, \quad R_x = \begin{bmatrix} 1 & 0 & 0 \\ 0 & \cos(\alpha_i) & -\sin(\alpha_i) \\ 0 & \sin(\alpha_i) & \cos(\alpha_i) \end{bmatrix} \quad (3.4)$$

The assigned frames must satisfy two conditions of the Denavit-Hartenberg method. These conditions are that the  $x_i$  axis is perpendicular to  $z_{i-1}$  and that the axis  $x_i$  must also intersect  $z_{i-1}$ . Assigning the coordinate frames for a manipulator can be achieved by many different assigned ways but such that the Denavit-Hartenberg conditions are satisfied.

### 3.2 Assigning the coordinate frames

The procedure of the Denavit-Hartenberg convention algorithm starts by assigning the coordinate frames to derive the forward kinematics equations of a manipulator. The process begins by choosing the z axes for the 7 joints by assign  $z_i$  to be the axis of actuation for joint  $i+1$ . Thus,  $z_0$  is the axis of actuation for joint 1,  $z_1$  is the axis of actuation for joint 2,  $z_2$  is the axis of actuation for joint 3,  $z_3$  is the axis of actuation for joint 4,  $z_4$  is the axis of actuation for joint 5,  $z_5$  is the axis of actuation for joint 6,  $z_6$  is the axis of actuation for joint 7,  $z_7$  is the axis of defining an important direction for the end-effector.

The base frame then established by choosing the origin  $o_0$  at any point on  $z_0$  as shown in Figure 3-2, the  $x_0$  and  $y_0$  axes are chosen to form a right-hand frame conveniently. The origins from  $o_1$  to  $o_7$  are chosen to be the points of the intersection between  $z_i$  and  $z_{i+1}$ . After that assigning the x axis from  $x_1$  to  $x_7$  where  $x_i$  must intersect and be perpendicular to the axis of  $z_{i-1}$  and  $z_i$ . The  $y_i$  axis established to form a right-hand frame, see Figure 3-2 below.

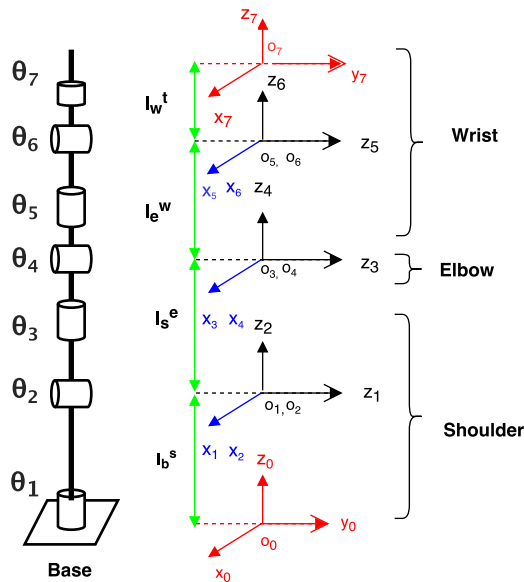


Figure 3-2: The coordinate frames assigned to the manipulator.

### 3.3 Forward kinematics equations

The forward kinematics equations can be obtained after assigning the coordinate frames and establishing the link parameters  $d_i$ ,  $a_i$ ,  $\alpha_i$  and  $\theta_i$  that form the D-H table. The link length  $a_i$  is distance along  $x_i$  from  $o_i$  to the intersection of the axis of  $x_i$  and the axis of  $z_{i-1}$ . From the assigned frames shown in Figure 3-2 there is no distance along any x axes from the origins to the point of intersection between the  $x_i$  and  $z_{i-1}$  so that the link length is zero in all the frames in the D-H table.

The link offset  $d_i$  is the distance along the axis  $z_{i-1}$  from the origin  $o_{i-1}$  to the intersection of the axis  $x_i$  and the axis of  $z_{i-1}$ . The assigned frames in Figure 3-2 shows that there are  ${}^b l_s$  along  $z_0$ ,  ${}^s l_e$  along  $z_2$ ,  ${}^e l_w$  along  $z_4$  and  ${}^w l_t$  along  $z_6$  while there is no any link offsets along  $z_1$ ,  $z_3$  and  $z_5$ .

The link twist  $\alpha_i$  is the angle between  $z_{i-1}$  and  $z_i$  measured about  $x_i$ . Figure 3-2 illustrates that about  $x_1$  there is an angle of  $-\frac{\pi}{2}$ (rad) between the axis of  $z_0$  and  $z_1$ , same angle is around the axes of  $x_3$  and  $x_5$ . The angle about  $x_2$  between the axes of  $z_1$  and  $z_2$  is  $\frac{\pi}{2}$ (rad), same angle around the axes of  $x_4$  and  $x_6$ . The figure shows that there is no angle around  $x_7$  between the axis of  $z_6$  and  $z_7$ .

The Link angle  $\theta_i$  is the angle between  $x_{i-1}$  and  $x_i$  measured about  $z_{i-1}$  since all the joints are revolute joints so the joint angles from  $\theta_1$  to  $\theta_7$  are variables. The Denavit-Hartenberg parameters are shown in Table 3.1

Table 3.1: Denavit-Hartenberg parameters

Joint	Link angle $\theta_i$ (rad)	Link twist $\alpha_i$ (rad)	Link length $a_i$ (mm)	Link offset $d_i$ (m)
1	$\theta_1$	$-\frac{\pi}{2}$	0	${}^b l_s=0.3$
2	$\theta_2$	$\frac{\pi}{2}$	0	0
3	$\theta_3$	$-\frac{\pi}{2}$	0	${}^s l_e=0.328$
4	$\theta_4$	$\frac{\pi}{2}$	0	0
5	$\theta_5$	$-\frac{\pi}{2}$	0	${}^e l_w=0.323$
6	$\theta_6$	$\frac{\pi}{2}$	0	0
7	$\theta_7$	0	0	${}^w l_t=0.0824$

The homogeneous transformation matrices  ${}^0 T_7$  are computed by substituting the above parameters into equation (3.2) for each joint. The resulting transformation

matrices are given below by equation (3.5). For the simplifications of the notations, the  $\cos(\theta_i)$  written as  $C_i$  and  $\sin(\theta_i)$  written as  $S_i$ .

$$\begin{aligned}
{}^0T_1 &= \begin{bmatrix} C_1 & 0 & -S_1 & 0 \\ S_1 & 0 & C_1 & 0 \\ 0 & -1 & 0 & {}^b l_s \\ 0 & 0 & 0 & 1 \end{bmatrix}, \quad {}^1T_2 = \begin{bmatrix} C_2 & 0 & S_2 & 0 \\ S_2 & 0 & -C_2 & 0 \\ 0 & 1 & 0 & 0 \\ 0 & 0 & 0 & 1 \end{bmatrix}, \quad {}^2T_3 = \begin{bmatrix} C_3 & 0 & -S_3 & 0 \\ S_3 & 0 & C_3 & 0 \\ 0 & 1 & 0 & {}^s l_e \\ 0 & 0 & 0 & 1 \end{bmatrix} \\
{}^3T_4 &= \begin{bmatrix} C_4 & 0 & -S_4 & 0 \\ S_4 & 0 & -C_4 & 0 \\ 0 & 1 & 0 & 0 \\ 0 & 0 & 0 & 1 \end{bmatrix}, \quad {}^4T_5 = \begin{bmatrix} C_5 & 0 & -S_5 & 0 \\ S_5 & 0 & C_5 & 0 \\ 0 & 1 & 0 & {}^e l_w \\ 0 & 0 & 0 & 1 \end{bmatrix}, \quad {}^5T_6 = \begin{bmatrix} C_6 & 0 & S_6 & 0 \\ S_6 & 0 & -C_6 & 0 \\ 0 & 1 & 0 & 0 \\ 0 & 0 & 0 & 1 \end{bmatrix} \\
{}^6T_7 &= \begin{bmatrix} C_7 & -S_7 & 0 & 0 \\ S_7 & C_7 & 0 & 0 \\ 0 & 1 & 0 & {}^w l_t \\ 0 & 0 & 0 & 1 \end{bmatrix}
\end{aligned} \tag{3.5}$$

The multiplications of the equations shown in (3.5) are performed using Symbolic Math Toolbox in MATLAB to obtain a symbolic form of the forward kinematic function  ${}^0T_7$  which gives the position and orientation of the end effector as a function of the joint angles  $\theta_i$ . The position and orientation transformation matrix of the end-effector relative to basis coordinate system is shown in equation (3.6).

$${}^0T_7 = {}^0T_1 {}^1T_2 {}^2T_3 {}^3T_4 {}^4T_5 {}^5T_6 {}^6T_7 = \begin{bmatrix} R_{11} & R_{12} & R_{13} & p_x \\ R_{21} & R_{22} & R_{23} & p_y \\ R_{31} & R_{32} & R_{33} & p_z \\ 0 & 0 & 0 & 1 \end{bmatrix} \tag{3.6}$$

Where  $R_{11}, R_{12}, R_{13}, R_{21}, R_{22}, R_{23}, R_{31}, R_{32}, R_{33}, p_x, p_y$  and  $p_z$  are given by the equations from (3.7) through (3.16) respectively.

$$\left. \begin{aligned} R_{11} = & C_7 S_6 (S_4 (S_1 S_3 - C_1 C_2 C_3) - \\ & C_1 C_4 S_2) C_6 (C_5 (C_4 (S_1 S_3 - C_1 C_2 C_3) + C_1 S_2 S_4) + S_5 (C_3 S_1 + C_1 C_2 S_3)) \\ & + S_7 (S_5 (C_4 (S_1 S_3 - C_1 C_2 C_3) + C_1 S_2 S_4) - C_5 (C_3 S_1 + C_1 C_2 S_3)) \end{aligned} \right\} \quad (3.7)$$

$$\left. \begin{aligned} R_{12} = & C_7 (S_5 (C_4 (S_1 S_3 - C_1 C_2 C_3) + C_1 S_2 S_4) - C_5 (C_3 S_1 + C_1 C_2 S_3)) - \\ & S_7 (S_6 (S_4 (S_1 S_3 - C_1 C_2 C_3) - C_1 C_4 S_2)) \\ & - C_6 (C_5 (C_4 (S_1 S_3 - C_1 C_2 C_3) + C_1 S_2 S_4) + S_5 (C_3 S_1 + C_1 C_2 S_3))) \end{aligned} \right\} \quad (3.8)$$

$$\left. \begin{aligned} R_{13} = & -C_6 (S_4 (S_1 S_3 - C_1 C_2 C_3) - C_1 C_4 S_2) - \\ & S_6 (C_5 (C_4 (S_1 S_3 - C_1 C_2 C_3) + C_1 S_2 S_4) + S_5 (C_3 S_1 + C_1 C_2 S_3)) \end{aligned} \right\} \quad (3.9)$$

$$\left. \begin{aligned} R_{21} = & -[C_7 (S_6 (S_4 (C_1 S_3 + C_2 C_3 S_1) + C_4 S_1 S_2) - C_6 (C_5 (C_4 (C_1 S_3 + \\ & C_2 C_3 S_1) - S_1 S_2 S_4) + S_5 (C_1 C_3 - C_2 S_1 S_3)))]] \\ & - S_7 (S_5 (C_4 (C_1 S_3 + C_2 C_3 S_1) - S_1 S_2 S_4) - C_5 (C_1 C_3 - C_2 S_1 S_3)) \end{aligned} \right\} \quad (3.10)$$

$$\left. \begin{aligned} R_{22} = & -[S_7 (S_6 (S_4 (C_1 S_3 + C_2 C_3 S_1) + C_4 S_1 S_2) - C_6 (C_5 (C_4 (C_1 S_3 + \\ & C_2 C_3 S_1) - S_1 S_2 S_4) + S_5 (C_1 C_3 - C_2 S_1 S_3)))]] \\ & - S_7 (S_5 (C_4 (C_1 S_3 + C_2 C_3 S_1) - S_1 S_2 S_4) - C_5 (C_1 C_3 - C_2 S_1 S_3)) \end{aligned} \right\} \quad (3.11)$$

$$R_{23} = C_6(S_4(C_1S_3 + C_2C_3S_1) + C_4S_1S_2) + \left. \begin{aligned} & S_6(C_5(C_4(C_1S_3 + C_2C_3S_1) - S_1S_2S_4) + S_5(C_1C_3 - C_2S_1S_3)) \end{aligned} \right\} \quad (3.12)$$

$$R_{33} = C_6(C_2C_4 - C_3S_2S_4) - S_6(C_5(C_2S_4 + C_3C_4S_2) - S_2S_3S_5) \left. \right\} \quad (3.13)$$

$$p_x = {}^s l_e C_1 S_2 - {}^w l_t (S_4(S_1 S_3 - C_1 C_2 C_3) - C_1 C_4 S_2) - \left. \begin{aligned} & [{}^w l_t (C_6(S_4(S_1 S_3 - C_1 C_2 C_3) - C_1 C_4 S_2) + S_6(C_5(C_4(S_1 \\ & S_3 - C_1 C_2 C_3) + C_1 S_2 S_4) + S_5(C_3 S_1 + C_1 C_2 S_3))))] \end{aligned} \right\} \quad (3.14)$$

$$p_y = [{}^w l_t (C_6(S_4(C_1 S_3 + C_2 C_3 S_1 + C_4 S_1 S_2) + S_6(C_5(C_4 \\ (C_1 S_3 + C_2 C_3 S_1) - S_1 S_2 S_4) + S_5(C_1 C_3 - C_2 S_1 S_3))))] \\ {}^e l_w (S_4(C_1 S_3 + C_2 C_3 S_1) + C_4 S_1 S_2) + {}^s l_e S_1 S_2 \left. \right\} \quad (3.15)$$

$$p_z = {}^b l_s + {}^e l_w (C_2 C_4 - C_3 S_2 S_4) - \left. \begin{aligned} & [({}^w l_t (S_6(C_5(C_2 S_4 + C_3 C_4 S_2) - S_2 S_3 S_5) - C_6(C_2 C_4 - C_3 S_2 S_4)) + {}^s l_e C_2)] \end{aligned} \right\} \quad (3.16)$$

where  ${}^b l_s$ ,  ${}^s l_e$ ,  ${}^e l_w$  and  ${}^w l_t$  are the given link offsets. After deriving these equations it is possible now to obtain the end-effector position and orientation from the individual joint angles. Tests for these equations and results will be shown in chapter 5.



# **Chapter 4**

## **Inverse Kinematics and Redundancy Resolution**

The inverse kinematics problem for a robot manipulator is defined as the problem of finding the values of the joint angles for a given position and orientation of the end-effector and the values of the geometric link parameters. The inverse kinematics technique is widely used for controlling the robot manipulators. It has finite number of solutions if the number of degrees of freedom of the arm are enough to perform a task in its reachable workspace. If the number of degrees of freedom of the manipulator are less than the required to perform a task by the end-effector, then the solutions are not available. However, if the number of degrees of freedom of the manipulators are greater than the required to perform a task such as for the redundant manipulator model in this study, then there are infinitely many solution.

For a redundant manipulator it is possible to generate an infinite number of joint trajectories that lead to the same end-effector desired trajectory. From these infinite number of solutions only one solution should be selected in order to control the manipulator. The redundancy resolution in redundant manipulators is referred to the problem of choosing one suitable solution from the infinite set of solutions. This selected solution must cause the end-effector to perform a task while satisfying additional constraints such as joint limit avoidance, control the elbow without changing the end-effector pose as well as avoiding the singularities and obstacles.

There are two different main methods for inverse kinematics, one solves the problem analytically at the position level and the other one solves it iteratively at the velocity level by approximating the solutions over time.

Solving the inverse kinematics and exploiting the redundancy at the position level will be used in this work. Chapter 2 discussed the advantages of exploiting the redundancy at the position level.

This chapter presents the redundancy parameterization methods [29] at the position level. Then the joint angles of the manipulator are calculated in term of a new defined arm angle. The relation between the joint angles and the arm angle then discussed. After that the joints limits avoidance has been presented. Lastly, the singular configurations are studied.

## 4.1 Redundancy parameterization

The manipulator model in this study has 7 joint angles while the given position and the orientations of the end-effector can be specified by six parameters meaning that one extra degree of freedom in the manipulator is available. The extra degree of freedom is representing the redundancy. This means that a combination of the joint angles can be freely changed independently from the placement of the end-effector [30]. This is so called the self-motion. For this reason a scalar parameter can be defined to represent this self-motion in order to allow specifying the joint angles values. Since the self-motion would not affect the end-effector placement, it can be chosen arbitrary with any value. However, developing a criteria for regulating this parameter can be used to attain some additional tasks such as avoiding the joints angle limit as well as avoiding the joints from passing through the singular configurations or performing some other additional tasks.

The redundancy parameterization and joint angles calculations used in this work are almost as in [29]. As shown in figure 4-1, if the end-effector is fixed, the wrist posture will be fixed as well. As long as the end-effector is stationary, it can be seen that the

elbow position can freely swivel about the axis connecting the shoulder and wrist; this is how the self-motion in this manipulator model appears.

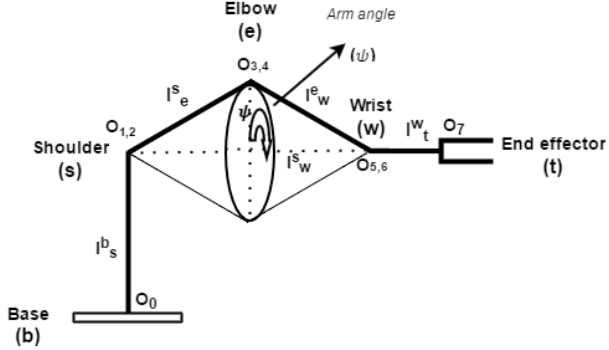


Figure 4-1: Arm angle definition.

The redundancy parametrization can be represented by an arm angle between a reference plane and arm plane [7]. The arm plane defined as the plane spanned by the shoulder, elbow and wrist. The reference plane can be determined by regarding the redundant manipulator as nonredundant by assuming joint 3 angle equal to zero so that the axis of the rotation in joint 2 and 4 are parallel. Thus, the plane spanned by the shoulder, elbow and wrist in this nonredundant arm can be regarded as a reference plane [29].

In this work the following notation is used:

${}^b l_s$  is the length from the base to the shoulder.

${}^s l_e$  is the length from the shoulder to the elbow.

${}^e l_w$  is the length from the elbow to the wrist.

${}^b P_7$  is the position of the end-effector.

${}^b R_7$  is the matrix defining the orientation of the end-effector.

The redundant degree of freedom that represents the self-motion of the manipulator is defined as the arm angle  $\psi$ .

Since the self-motion of the arm is a free rotation around the axis connecting the shoulder and wrist, this axis must be defined. Let  ${}^s L_w$  be the vector between the

centers of the shoulder and wrist. The wrist position  $w$  can be calculated by (4.1).

$$w = \begin{bmatrix} w_x \\ w_y \\ w_z \end{bmatrix} = {}^bP_7 - {}^w l_t {}^bR_7 \begin{bmatrix} 0 \\ 0 \\ 1 \end{bmatrix} \quad (4.1)$$

Where the  ${}^bP_7$  and  ${}^bR_7$  are the given position and orientation of the end-effector respectively.  ${}^w l_t$  is the length from the wrist to the end-effector rotating around z-axis. Equation (4.1) gives the wrist position with respect to the base. Calculating the wrist position with respect to the shoulder can be computed as shown in equation (4.2).

$${}^sL_w = w - {}^bL_s \quad (4.2)$$

where  $w$  is given by (4.1) and  ${}^bL_s$  is the vector between the centers of the base and the shoulder rotating around z axis given by (4.3).

$${}^bL_s = \begin{bmatrix} 0 \\ 0 \\ {}^b l_s \end{bmatrix} \quad (4.3)$$

From the given pose, the end-effector is fixed then the wrist position is also fixed as mentioned before. Thus, the line between shoulder and wrist,  ${}^sL_w$  is constant because all variables in the right-side in (4.2) are constants for stationary end-effector.

A rotation matrix needs to be derived to representing the freely rotation arm angle  $\psi$  around the line connecting the shoulder and wrist axis as shown in figure 4-1. Rodrigues formula is an efficient algorithm for representing a rotating vector in space, given an axis  ${}^sL_w$  and angle of rotation  $\psi$  [31]. The Rodrigues formula for the rotational matrix is given by (4.4).

$$R_\psi = I + (1 - \cos(\psi)){}^s k_w^2 + \sin(\psi){}^s k_w \quad (4.4)$$

Where I is the  $3 \times 3$  identity matrix and  ${}^s k_w$  is a skew symmetric matrix of  ${}^s u_w$  which

is given by (4.5).

$${}^s k_w = \begin{pmatrix} 0 & -{}^s u_w(z) & {}^s u_w(y) \\ {}^s u_w(z) & 0 & -{}^s u_w(x) \\ -{}^s u_w(y) & {}^s u_w(x) & 0 \end{pmatrix} \quad (4.5)$$

where  ${}^s u_w(x)$ ,  ${}^s u_w(y)$  and  ${}^s u_w(z)$  are the x,y and z coordinates of the vector  ${}^s u_w$ .

The  ${}^s u_w$  is the unit vector defining direction of  ${}^s L_w$ , which is given by (4.6).

$${}^s u_w = \frac{{}^s L_w}{\| {}^s L_w \|} \quad (4.6)$$

where  $\| {}^s L_w \|$  is the norm (or length) of  ${}^s L_w$ .

As mentioned before chosen any arm angle would not effect the wrist position. However, it can be seen that the wrist spherical joint orientation viewed from the base of the manipulator is changing for different arm angles. The joint 4 angle is independent from the defined arm angle. However, changing the arm angle leads to change the shoulder spherical joint orientation, which can be calculated as follows

$${}^0 R_3 = R_\psi {}^0 R'_3 \quad (4.7)$$

where  ${}^0 R'_3$  is the shoulder rotation matrix when the joint 3 angle is assumed to be zero (reference plane). The arm angle is zero if and only if the arm plane coincides with the reference plane.

## 4.2 Joint angles computations

This section presents the methods for computing the seven joint angles using the new defined arm angle based on the redundancy parameterization method discussed in the previous section.

### 4.2.1 Elbow joint angle ( $\theta_4$ )

From figure (4-1) it can be seen that in the redundancy circle choosing any arm angle will not affect the elbow joint angle 4 so that for any fixed end-effector the elbow joint angle 4 can be calculated. As shown in figure 4-2, the cosine law can be applied

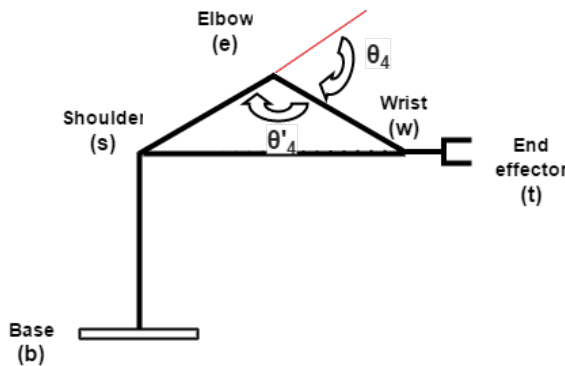


Figure 4-2: Joint angle 4 calculation.

to calculate joint 4 prime ( $\theta_4'$ ) as in(4.8).

$$\| {}^s L_w \|^2 = {}^s l_e^2 + {}^e l_w^2 - 2 {}^s l_e {}^e l_w \cos(\theta_4') \quad (4.8)$$

From this equation  $\cos(\theta_4')$  can be derived as following

$$\cos(\theta_4') = \frac{{}^s l_e^2 + {}^e l_w^2 - \| {}^s L_w \|^2}{2 {}^s l_e {}^e l_w} \quad (4.9)$$

Where  $\| {}^s L_w \|^2$  is the length of the vector in (4.2). From this equation it is possible to calculate  $\theta_4$  by (4.10).

$$\theta_4 = \pi - \theta_4' \quad (4.10)$$

#### 4.2.2 Shoulder joint angles ( $\theta_1$ , $\theta_2$ and $\theta_3$ )

The shoulder joint angles depend on the defined arm angle as shown in equation (4.7). Varying the arm angle will generate different values for  $\theta_1, \theta_2$  and  $\theta_3$  with the same given posture of end-effector. Calculating the shoulder joint angles in term of the arm angle requires first to find the reference plane. From the redundancy parameterization definition, the reference plane is the plane containing the shoulder, elbow, wrist when the joint angle 3 is equal to zero.

Let  $\theta_1', \theta_2'$  and  $\theta_3'$  are the joint angles for the reference plane associated with the rotation matrix  ${}^0R'_3$ . The redundant manipulator becomes non-redundant by fixing  $\theta_3'=0$ .

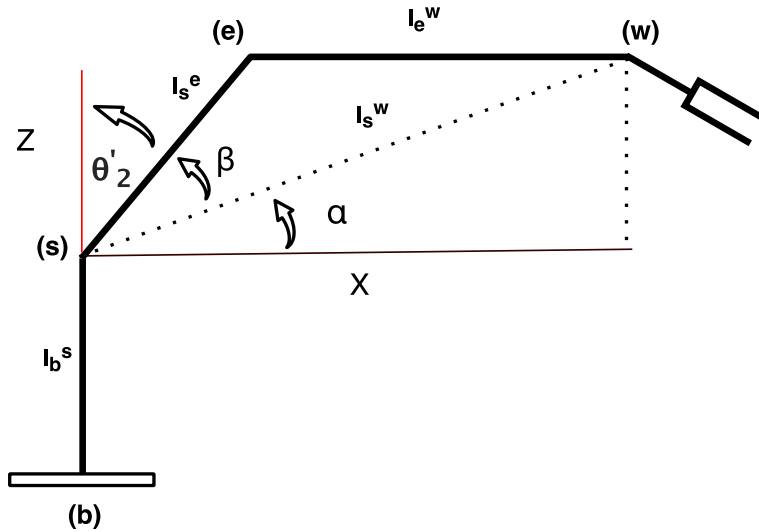


Figure 4-3: The reference joint angles calculation.

It can be noted that from the known projection of the wrist position onto the horizontal plane, the  $\theta_1'$  can be calculated as follows

$$\theta_1' = \text{atan2}(w_y, w_x) \quad (4.11)$$

Where  $w_x$  and  $w_y$  are the x and y coordinates of the vector given in (4.1). The figure

4-3 shows that the  $\theta_2'$  can be calculated by the following equation

$$\theta_2' = \frac{\pi}{2} - \alpha - \beta \quad (4.12)$$

Where  $\alpha$  given by (4.13) and  $\beta$  given by (4.14)

$$\alpha = \sin^{-1} \left( \frac{w_z - {}^b l_s}{\| {}^s L_w \|} \right) \quad (4.13)$$

Where  $w_z$  is the z coordinate of the vector calculated by (4.1). The angle  $\beta$  can be calculated using cosine law as shown in figure 4-3.

$$\beta = \cos^{-1} \left( \frac{{}^s l_e^2 + \| {}^s L_w \|^2 - {}^e l_w^2}{2 {}^s l_e \| {}^s L_w \|} \right) \quad (4.14)$$

After computing  $\theta_1'$  and  $\theta_2'$  using (4.11) and (4.12) respectively and knowing that  $\theta_3'$  equals to zero it is now possible to compute  ${}^0 R'_3$  using the rotation matrix

$${}^{i-1} R'_i = \begin{bmatrix} \cos(\theta'_i) & -\sin(\theta'_i) \cos(\alpha_i) & \sin(\theta'_i) \sin(\alpha_i) \\ \sin(\theta'_i) & \cos(\theta'_i) \cos(\alpha_i) & -\cos(\theta'_i) \sin(\alpha_i) \\ 0 & \sin(\alpha_i) & \cos(\alpha_i) \end{bmatrix} \quad (4.15)$$

Substituting the values of  $\theta_1'$ ,  $\theta_2'$  and  $\theta_3' = 0$  into (4.15) with the parameters of the first three joints listed in D-H table in chapter 3, will give the following equations in (4.16)

$${}^0 R'_1 {}^1 R'_2 {}^2 R'_3 = \quad (4.16)$$

$$\begin{bmatrix} C_{\theta'_1} & 0 & -S_{\theta'_1} \\ S_{\theta'_1} & 0 & C_{\theta'_1} \\ 0 & -1 & 0 \end{bmatrix} \begin{bmatrix} C_{\theta'_2} & 0 & S_{\theta'_2} \\ S_{\theta'_2} & 0 & -C_{\theta'_2} \\ 0 & 1 & 0 \end{bmatrix} \begin{bmatrix} 1 & 0 & 0 \\ 0 & 0 & 1 \\ 0 & -1 & 0 \end{bmatrix}$$

Where  ${}^0 R'_1$ ,  ${}^1 R'_2$  and  ${}^2 R'_3$  the rotation matrix of the reference joint angles.

Now the matrix  ${}^0 R'_3$  can be calculated as follows

$$\begin{aligned}
{}^0R'_3 &= {}^0R'_1 {}^1R'_2 {}^2R'_3 \\
&= \begin{bmatrix} C_{\theta'_1}C_{\theta'_2} & -C_{\theta'_1}S_{\theta'_1} & -S_{\theta'_1} \\ C_{\theta'_2}S_{\theta'_1} & -S_{\theta'_1}S_{\theta'_2} & C_{\theta'_1} \\ -S_{\theta'_2} & -C_{\theta'_2} & 0 \end{bmatrix}
\end{aligned} \tag{4.17}$$

This matrix is constant for any given pose. Now it is possible to calculate the shoulder joint angles in term of the arm angle by substituting the equations (4.4) and (4.17) into (4.7), this will result in the following equation

$${}^0R_3 = \sin(\psi){}^sk_w {}^0R'_3 - \cos(\psi)({}^sk_w^2) {}^0R'_3 + (I + {}^sk_w^2) {}^0R'_3 \tag{4.18}$$

In the right-hand side in equation (4.18), the  ${}^sk_w$  is given by (4.5) and  ${}^0R'_3$  is given by (4.17) so the shoulder joint angles  $\theta_1, \theta_2$  and  $\theta_3$  in term of the arm angle  $\psi$  are given by (4.18). For mathematical simplifications in equation (4.18), it can be rewritten as follows

$${}^0R_3 = \sin(\psi)X_s + \cos(\psi)Y_s + Z_s \tag{4.19}$$

Where the matrices  $X_s, Y_s$  and  $Z_s$  are given constant matrices defined by (4.20), (4.21) and (4.22) respectively.

$$X_s = {}^sk_w {}^0R'_3 = \begin{bmatrix} X_{s11} & X_{s12} & X_{s13} \\ X_{s21} & X_{s22} & X_{s23} \\ X_{s31} & X_{s32} & X_{s33} \end{bmatrix} \tag{4.20}$$

$$Y_s = -({}^sk_w^2) {}^0R'_3 = \begin{bmatrix} Y_{s11} & Y_{s12} & Y_{s13} \\ Y_{s21} & Y_{s22} & Y_{s23} \\ Y_{s31} & Y_{s32} & Y_{s33} \end{bmatrix} \tag{4.21}$$

$$Z_s = (I + {}^sk_w^2) {}^0R'_3 = \begin{bmatrix} Z_{s11} & Z_{s12} & Z_{s13} \\ Z_{s21} & Z_{s22} & Z_{s23} \\ Z_{s31} & Z_{s32} & Z_{s33} \end{bmatrix} \tag{4.22}$$

Equation (4.19) can be written in the matrix form in order to compute the shoulder joint angles easily by comparing the matrices elements in the right-hand side and left-hand side of this equation.  ${}^0R_3$  matrix can be computed by substituting the parameters of the shoulder joints in the D-H table in chapter 3 into (4.15) which will give the matrix form in (4.23).

$${}^0R_3 = \begin{bmatrix} C_1C_2C_3 - S_1S_3 & -C_1S_2 & -C_3S_1 - C_1C_2S_3 \\ C_1S_3 + C_2C_3S_1 & -S_1S_2 & C_1C_3 - C_2C_1S_3 \\ -S_2C_3 & -C_2 & S_2S_3 \end{bmatrix} \quad (4.23)$$

The right hand-side in (4.19) can be written in the following matrix form as shown in (4.24).

$${}^0R_3 = \begin{bmatrix} S_\psi X_{s11} + C_\psi Y_{s11} + Z_{s11} & S_\psi X_{s12} + C_\psi Y_{s12} + Z_{s12} & S_\psi X_{s13} + C_\psi Y_{s13} + Z_{s13} \\ S_\psi X_{s21} + C_\psi Y_{s21} + Z_{s21} & S_\psi X_{s22} + C_\psi Y_{s22} + Z_{s22} & S_\psi X_{s23} + C_\psi Y_{s23} + Z_{s23} \\ S_\psi X_{s31} + C_\psi Y_{s31} + Z_{s31} & S_\psi X_{s32} + C_\psi Y_{s32} + Z_{s32} & S_\psi X_{s33} + C_\psi Y_{s33} + Z_{s33} \end{bmatrix} \quad (4.24)$$

Where  $S_\psi$  and  $C_\psi$  are short-cuts for  $\sin(\psi)$  and  $\cos(\psi)$  respectively. By equating the elements of (4.23) and (4.24), it is possible to calculate the shoulder joint angles. The joint angle  $\theta_1$  can be computed by comparing  ${}^0R_3(1, 2)$  and  ${}^0R_3(2, 2)$  as the following equation illustrates

$$\frac{-S_{\theta_1}S_{\theta_2}}{-C_{\theta_1}S_{\theta_2}} = \frac{S_\psi X_{s22} + C_\psi Y_{s22} + Z_{s22}}{S_\psi X_{s12} + C_\psi Y_{s12} + Z_{s12}} \quad (4.25)$$

This equation can be rewritten as the following equation in (4.26) which parametrizes the joint angle  $\theta_1$  in term of the arm angle  $\psi$ .

$$\theta_1 = \text{atan} \left( \frac{-S_\psi X_{s22} - C_\psi Y_{s22} - Z_{s22}}{-S_\psi X_{s12} - C_\psi Y_{s12} - Z_{s12}} \right) \quad (4.26)$$

Similarly comparing  ${}^0R_3(3, 2)$  in (4.23) and (4.24) can be used to compute the joint angle  $\theta_2$  as follows

$$-C_{\theta_2} = S_\psi X_{s32} + C_\psi Y_{s32} + Z_{s32} \quad (4.27)$$

This equation can be rewritten as the following:

$$\theta_2 = \arccos(-S_\psi X_{s32} - C_\psi Y_{s32} - Z_{s32}) \quad (4.28)$$

In the same way comparing  ${}^0R_3(3,1)$  and  ${}^0R_3(3,3)$  in (4.23) and (4.24) one obtains

$$\frac{S_{\theta_2} S_{\theta_3}}{-S_{\theta_2} C_{\theta_3}} = \frac{S_\psi X_{s33} + C_\psi Y_{s33} + Z_{s33}}{S_\psi X_{s31} + C_\psi Y_{s31} + Z_{s31}} \quad (4.29)$$

Simplifying equation (4.29) one can calculate the joint angle  $\theta_3$  as shown in equation (4.30).

$$\theta_3 = \arctan \left( \frac{S_\psi X_{s33} + C_\psi Y_{s33} + Z_{s33}}{-S_\psi X_{s31} - C_\psi Y_{s31} - Z_{s31}} \right) \quad (4.30)$$

So equations (4.26), (4.28) and (4.30) give the shoulder joint angles  $\theta_1$ ,  $\theta_2$  and  $\theta_3$  as function of the new defined arm angle  $\psi$ .

### 4.2.3 Wrist joint angles ( $\theta_5$ , $\theta_6$ and $\theta_7$ )

This section discuss the computations of the wrist joint angles  $\theta_5$ ,  $\theta_6$  and  $\theta_7$ . It is clear that the given orientation of the end-effector  ${}^bR_7$  with respect to the base can be calculated by the following equation

$${}^bR_7 = {}^0R_3 {}^3R_4 {}^4R_7 \quad (4.31)$$

This equation can be rewritten in term of the arm angle as shown in (4.32).

$${}^4R_7 = ({}^3R_4)^T ({}^0R_3)^T {}^bR_7 \quad (4.32)$$

Where  ${}^0R_3$  is given by (4.7) and  ${}^3R_4$  is given by substituting the elbow joint  $\theta_4$  computed by (4.10) and the link parameters of the joint 4 from D-H table in chapter 3 into (4.15). Then  ${}^4R_7$  can be written as the following

$${}^4R_7 = \sin(\psi)X_w + \cos(\psi)Y_w + Z_w \quad (4.33)$$

Where  $X_w$ ,  $Y_w$  and  $Z_w$  are constant matrices for a any given pose. These matrices are defined by

$$X_w = ({}^3R_4)^T ({}^s k_w)^T ({}^0R'_3)^T = \begin{bmatrix} X_{w11} & X_{w12} & X_{w13} \\ X_{w21} & X_{w22} & X_{w23} \\ X_{w31} & X_{w32} & X_{w33} \end{bmatrix} \quad (4.34)$$

$$Y_w = -({}^3R_4)^T ({}^s k_w^2)^T ({}^0R'_3)^T = \begin{bmatrix} Y_{w11} & Y_{w12} & Y_{w13} \\ Y_{w21} & Y_{w22} & Y_{w23} \\ Y_{w31} & Y_{w32} & Y_{w33} \end{bmatrix} \quad (4.35)$$

$$Z_w = ({}^3R_4)^T (I + {}^s k_w^2)^T ({}^0R'_3)^T = \begin{bmatrix} Z_{w11} & Z_{w12} & Z_{w13} \\ Z_{w21} & Z_{w22} & Z_{w23} \\ Z_{w31} & Z_{w32} & Z_{w33} \end{bmatrix} \quad (4.36)$$

Similar to the way of calculating the shoulder joint variables, the wrist joint vari-

ables can be calculated. Equation (4.33) can be written in matrix form in order to compute the wrist joint angles easily by comparing the matrices in the right and left sides of the equation.  ${}^4R_7$  matrix can be computed by substituting the parameters of the wrist joints in the D-H table in chapter 3 into (4.15) which will give the following matrix form

$${}^4R_7 = \begin{bmatrix} C_5C_6C_7 - S_5S_7 & -C_7S_5 - C_5C_6S_7 & -C_5S_6 \\ C_5S_7 + C_6C_7S_5 & C_5C_7 - C_6S_5S_7 & S_5S_6 \\ -S_6C_7 & S_6S_7 & C_6 \end{bmatrix} \quad (4.37)$$

The right-hand side of (4.33) can be written as follows

$${}^4R_7 = \begin{bmatrix} S_\psi X_{w11} + C_\psi Y_{w11} + Z_{w11} & S_\psi X_{w12} + C_\psi Y_{w12} + Z_{w12} & S_\psi X_{w13} + C_\psi Y_{w13} + Z_{w13} \\ S_\psi X_{w21} + C_\psi Y_{w21} + Z_{w21} & S_\psi X_{w22} + C_\psi Y_{w22} + Z_{w22} & S_\psi X_{w23} + C_\psi Y_{w23} + Z_{w23} \\ S_\psi X_{w31} + C_\psi Y_{w31} + Z_{w31} & S_\psi X_{w32} + C_\psi Y_{w32} + Z_{w32} & S_\psi X_{w33} + C_\psi Y_{w33} + Z_{w33} \end{bmatrix} \quad (4.38)$$

Where  $S_\psi$  and  $C_\psi$  denote  $\sin(\psi)$  and  $\cos(\psi)$  respectively. By comparing the elements of (4.37) and (4.38), it is possible to calculate the wrist joint angles. The joint angle  $\theta_5$  can be computed by comparing  ${}^4R_7(1, 3)$  and  ${}^4R_7(2, 3)$  as following

$$\frac{S_{\theta_5}S_{\theta_6}}{-C_{\theta_5}S_{\theta_6}} = \frac{S_\psi X_{w23} + C_\psi Y_{w23} + Z_{w23}}{S_\psi X_{w13} + C_\psi Y_{w13} + Z_{w13}} \quad (4.39)$$

This equation can be rewritten as the following equation in (4.40), which parametrizes the joint angle  $\theta_5$  in term of the arm angle  $\psi$ .

$$\theta_5 = \tan^{-1} \left( \frac{S_\psi X_{w23} + C_\psi Y_{w23} + Z_{w23}}{S_\psi X_{w13} + C_\psi Y_{w13} + Z_{w13}} \right) \quad (4.40)$$

Similarly comparing  ${}^4R_7(3, 3)$  in (4.37) and (4.38) can be used to compute the joint angle  $\theta_6$  as the following

$$S_{\theta_6} = S_\psi X_{w33} + C_\psi Y_{w33} + Z_{w33} \quad (4.41)$$

This equation can be written in the following form

$$\theta_6 = \cos^{-1}(S_\psi X_{w33} + C_\psi Y_{w33} + Z_{w33}) \quad (4.42)$$

In the same way comparing  ${}^4R_7(3, 2)$  and  ${}^4R_7(3, 1)$  in (4.37) and (4.38) can be used to compute joint angle  $\theta_7$  as shown in equation (4.43).

$$\frac{S_{\theta_6} S_{\theta_7}}{-S_{\theta_6} C_{\theta_7}} = \frac{S_\psi X_{w32} + C_\psi Y_{w32} + Z_{w32}}{S_\psi X_{w31} + C_\psi Y_{w31} + Z_{w31}} \quad (4.43)$$

Simplifying equation (4.43) as follows

$$\theta_7 = \tan^{-1} \left( -\frac{S_\psi X_{w32} + C_\psi Y_{w32} + Z_{w32}}{S_\psi X_{w31} + C_\psi Y_{w31} + Z_{w31}} \right) \quad (4.44)$$

So far the seven joint angles of the manipulator have been calculated in term of the new arm angle parameter  $\psi$ . The next section will discuss the effect of changing the arm angle on the joint angles.

### 4.3 The effect of the arm angle on the joint angles

The previous section presents the relation between the joint angles and the defined arm angle. The arm angle can be chosen arbitrary for any given pose when there are no additional constraints. This section study how varying the arm angle would affect the joint angles. As mentioned before, the arm angle has influence on the shoulder and wrist joints while the elbow joint has no impact caused by variations of the arm angle. The values of derivatives define the instantaneous rate of change of a quantity with respect to another quantity. It gives information about the slope of the tangent line to the graph of any function; for this reasons the differentiation can be used to study the rate of change of the shoulder or wrist joints with respect to the arm angle [32]. The joint angles 1, 3, 5 and 7 are given in term of the arm angle as a tangent functions as shown in equations (4.26), (4.30), (4.40) and (4.44) respectively. Since these joint angles are given in the same form, one general function only can be studied and the same results can be apply to all these joint angles functions. The general tangent function form for joints 1, 3, 5 and 7 can be written as follows

$$\theta = \tan^{-1} \left( \frac{S_\psi X_n + C_\psi Y_n + Z_n}{S_\psi X_d + C_\psi Y_d + Z_d} \right) \quad (4.45)$$

Where  $S_\psi$  and  $C_\psi$  denoted the  $\sin(\psi)$  and  $\cos(\psi)$  respectively.  $n$  marks numerator coefficients and  $d$  marks denominator coefficients. Differentiating the inverse tangent, equation (4.45) can be derived in the following form

$$\frac{d\theta}{d\psi} = \frac{d}{d\psi} (\tan^{-1} f(\psi)) = \frac{1}{1 + f(\psi)^2} \frac{d}{d\psi} f(\psi) \quad (4.46)$$

The results of differentiating equation (4.45) with respect to the arm angle  $\psi$  can be written as

$$\frac{d\theta}{d\psi} = \frac{S_\psi x + C_\psi y + z}{(S_\psi X_n + C_\psi Y_n + Z_n)^2 + (S_\psi X_d + C_\psi Y_d + Z_d)^2} \quad (4.47)$$

where x, y and z are given by the following equations respectively.

$$x = Y_d Z_n - Y_n Z_d \quad (4.48)$$

$$y = X_n Z_d - X_d Z_n \quad (4.49)$$

$$z = X_n Y_d - X_d Y_n \quad (4.50)$$

The differentiation can be used to finds the points associated with maximum and minimum values of a function looking at the point where the slope is zero. Using the first derivative of the equation (4.45), it is possible to investigate whether there are critical arm angles at which the joint angles are maximum and minimum or if there are no critical arm angles, this can be studied by setting equation (4.47) equal to zero where  $\frac{d\theta}{d\psi} = 0$ . This will help in avoiding the joint limits as will be discussed in the next section. By setting equation (4.47) equal to zero, one obtains

$$S_\psi x + C_\psi y + z = 0$$

Solving this equation to find the critical values of  $\psi$  can be done using the Weierstrass substitution method which is the tangent half-angle substitution

$$u = \tan(\frac{\psi}{2}) \quad \text{then} \quad \sin(\psi) = \frac{2u}{u^2+1} \quad \text{and} \quad \cos(\psi) = \frac{1-u^2}{u^2+1}$$

After substituting and solving the equation, two critical arm angles are obtained where the joint angle is either maximum or minimum for each cyclic period as follows

$$\psi_1 = 2 \tan^{-1} \left( \frac{x - \sqrt{x^2 + y^2 - z^2}}{y - z} \right) \quad (4.51)$$

$$\psi_2 = 2 \tan^{-1} \left( \frac{x + \sqrt{x^2 + y^2 - z^2}}{y - z} \right) \quad (4.52)$$

The arm angle as discussed in the previous section is the angle between the reference plane and the arm plane rotating around the line connecting the shoulder and wrist so that the arm angle move in circular form, the range of the arm angle can be limited to  $360^\circ$  knowing that this does not lose any valid solutions of the arm angle

because it is repeatable for each full rotation around the line connecting the shoulder and the wrist for the given pose. So the critical arm angles where the joint angles are either maximum or minimum are given by the equations (4.51) and (4.52). It is worth to note that these two arm angles can only be obtained if the following inequality is satisfied.

$$x^2 + y^2 - z^2 > 0 \quad (4.53)$$

Otherwise there are no critical arm angles. This condition implies that it is possible to check the profile of each joint angle(1, 3, 5 or 7) since all the variables in (4.53) can be calculated by (4.48), (4.49) and (4.50) from the given pose of the end-effector.

Figure 4-4 illustrates an example of the profile of the tangent joint angles with respect to the arm angle when the condition in (4.53) is satisfied. The figure shows that the profile have cyclic form and the joint angle is the same at any arm angle  $\psi$  and  $\psi \pm 360^\circ$  meaning that manipulator would have the same configuration at these arm angles. The sign of the first derivative in this case is changing between minus and plus meaning that the dependence profile of the joint is either increasing or decreasing.

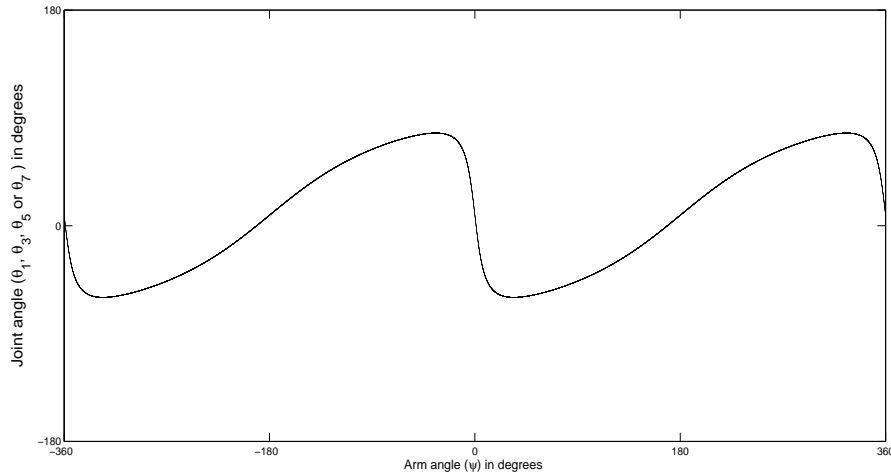


Figure 4-4: Example profile of the joint angles  $\theta_1$ ,  $\theta_3$ ,  $\theta_5$  or  $\theta_7$  with respect to the redundancy parameter when (4.53) is satisfied.

One of the arm angles obtained by (4.51) and (4.52) gives maximum and the other one gives minimum. The second derivative can be used to distinguish between the maximum and minimum points by checking the sign of the coefficient of the second derivative function. If the second derivative is positive  $\frac{d^2\theta}{d\psi^2} > 0$ , then the joint angle at this arm angle is minimum and if the second derivative is negative  $\frac{d^2\theta}{d\psi^2} < 0$ , then the joint angle at this arm angle is maximum. Differentiating equation (4.47) will give the second derivative of equation (4.45) as the following

$$\frac{d^2\theta}{d\psi^2} = \frac{C_\psi x - S_\psi y}{(n^2 + d^2)} - \frac{2(S_\psi x + C_\psi y + z)[(X_d C_\psi - Y_d S_\psi)d + (X_n C_\psi - Y_n S_\psi)n]}{(n^2 + d^2)^2} \quad (4.54)$$

where

$$n = S_\psi X_n + C_\psi Y_n + Z_n$$

$$d = S_\psi X_d + C_\psi Y_d + Z_d$$

So the sign of (4.54) defines whether the arm angle gives maximum or minimum, which will be used to avoid the joint limits as next section discuss.

Sometimes the condition in (4.53) is not satisfied meaning the following

$$x^2 + y^2 - z^2 < 0 \quad (4.55)$$

In this case there are no critical arm angles where the joint angles are maximum or minimum, for this reason the profile of the tangent function is monotonically increasing or decreasing on some certain arm angle ranges. Figure 4-5 shows an example of increasing joint angle with no critical arm angle. The figure shows also that the joint angle is the same at any arm angle  $\psi$  and  $\psi \pm 360^\circ$ . The sign of the first derivative function in this case is positive or negative meaning that the profile of the joint is increasing or decreasing.

In summary for the joint angles 1, 3, 5 and 7 if the conditions in (4.53) is satisfied for any of them, then the profile of the function is cyclic. However, if the condition in (4.55) is satisfied then the profile of the joint angle with respect to the arm angle is continue to increase or decrease on some arm angle ranges. If the conditions in (4.53)

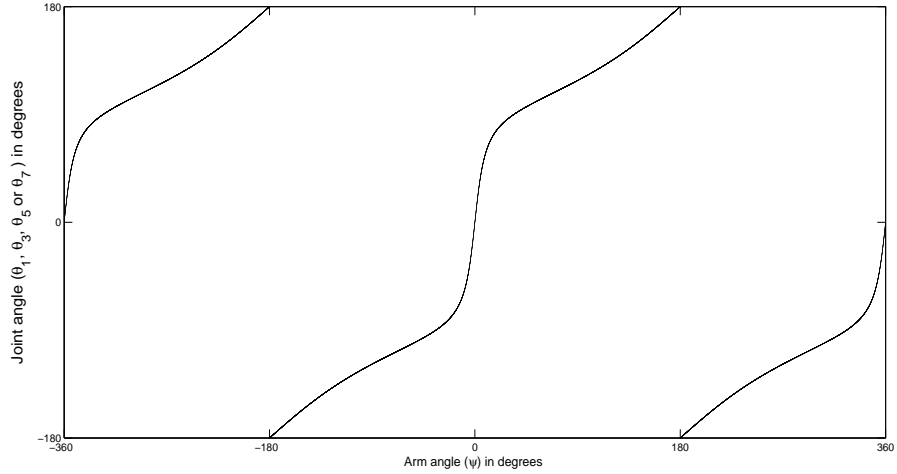


Figure 4-5: Example profile of the joint angles  $\theta_1$ ,  $\theta_3$ ,  $\theta_5$  or  $\theta_7$  with respect to the redundancy parameter when (4.55) is satisfied.

and (4.55) are not satisfied, it means that the joint angle at a singular configuration as it will be discussed in the next section. This study between the defined arm angle and the other joint angles will be used in the methods of avoiding the joint angles limits as it will be presented in the next section.

Previously the tangent type joint angles (1, 3, 5 and 7) were studied. Now the cosine type joint angle (2 and 6) will be discussed. Equations (4.27) and (4.41) can be written in a general form for both of them to investigate the impact of changing the arm angle on these joint angles as the following equation shows

$$C_\theta = S_\psi x_c + C_\psi y_c + z_c \quad (4.56)$$

Where the constants  $x_c$ ,  $y_c$  and  $z_c$  are calculated from the given pose as explained before, , see equations (4.20)-(4.22) for (4.27) and (4.34)-(4.36) for (4.41), respectively.

The  $S_\psi$  and  $C_\psi$  denote  $\sin(\psi)$  and  $\cos(\psi)$  respectively.

The critical arm angles where the profile of the joint angle has significant changes whether as a turning point from maximum to minimum or contrary, can be obtained

using the first derivative of (4.56). Differentiating this equation with respect to the arm angle  $\psi$  gives the following

$$\frac{d\theta}{d\psi} = \frac{S_\psi y_c - C_\psi x_c}{S_\theta} \quad (4.57)$$

Setting (4.57) equal to zero where  $\frac{d\theta}{d\psi} = 0$  to find the critical arm angle. In order for equation (4.57) to be zero, the numerator must be equal to zero while  $S(\theta)$  in the denominator is not equal zero otherwise, if the denominator is equal to zero it will lead to the algorithmic singularity, next section will discuss tackling this problem. When the numerator in (4.57) equal to zero, the following critical arm angle is obtained

$$\psi_c = \tan^{-1} \left( \frac{x_c}{y_c} \right) \quad (4.58)$$

This arm angle is a critical point where the gradient of the profile of the joint angle is turning from decreasing to increasing or turning from increasing to decreasing, meaning that at this arm angle the joint angle either maximum or minimum. Knowing where the joint angles are at their peaks used to avoid the joint limits. Figure 4-6 shows an example of the profile for the joint (2 or 6). These joints, which have cosine form dependence, are always cyclic and the critical arm angles are always  $180^\circ$  apart from each other. The joint angles are the same at any arm angle  $\psi$  and  $\psi \pm 360^\circ$ .

The first derivative in (4.57) can be used to distinguish whether the joint angle at the critical arm angle in (4.58) is maximum or minimum. It is possible to check this using the first derivative sign changes before and after this turning point. Let the symbol  $\epsilon$  represents a small quantity value to the right and left of  $\psi_c$  as  $[\psi_c \pm \epsilon]$ . If the sign of equation (4.57) changed from minus to plus, the arm angle is minimum in this case as shown in table 4.1. However, if it changes from plus to minus, the arm angle is maximum as shown in table 4.2.

So far we have calculated one arm angle which maybe maximum or minimum. From the cosine profile behaviour shown in figure 4-6 there is always two another turning points can be calculated easily because they are apart from  $\psi_c$  by  $180^\circ$  for

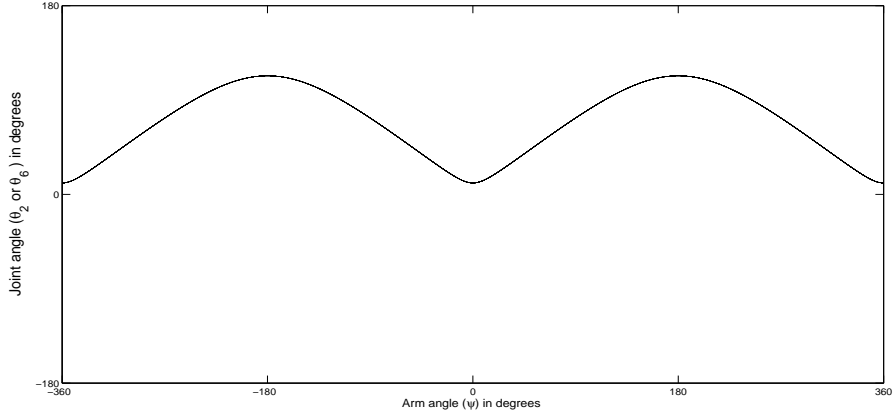


Figure 4-6: Example profile of the joint angles  $\theta_2$  or  $\theta_6$  with respect to the redundancy parameter where  $\theta \neq 0^\circ$  and  $\theta \neq 180^\circ$ .

Table 4.1:  $\psi_c$  is minimum

The value	$\psi_c - \epsilon$	$\psi_c$	$\psi_c + \epsilon$
Sign of (4.57)	-	0	+
Shape of the graph	↘	→	↗

Table 4.2:  $\psi_c$  is maximum

The value	$\psi_c - \epsilon$	$\psi_c$	$\psi_c + \epsilon$
Sign of (4.57)	+	0	-
Shape of the graph	↗	→	↘

each periodic cycle [29], this is what can be realized from figure 4-6. In summary there are  $\psi_c$  and  $\psi_c \pm 180^\circ$  within the range  $360^\circ$ . If  $\psi_c$  is maximum then  $\psi_c \pm 180^\circ$  are minimum critical arm angle and the other way around.

## 4.4 Redundancy resolution for joint limits

This section discuss how the available redundancy in the manipulator can be used to avoid the joint angles limits. As mentioned before there are infinitely many joint trajectories that perform the same task by the end-effector in the redundant manipulators workspace. All these solutions are acceptable if there are no constraints such as joint limits or obstacles in the working environment. However, due to the joint limits, some of these solutions have to be avoided in order not to violate the constraints of the joint limits. The problem of avoiding the joint limits can be done by regulating the new defined arm angle that discussed in the previous section. It is possible by trial-and-error to choose the arm angle and check if the obtained joint angles are inside the allowable range for each particular joint. However, this is not a practical solution for the real-time applications, therefore, there is a necessity for developing an automated process of choosing a proper arm angle that makes the joint angles stay inside the permissible joints domain. As shown in the procedure of defining the arm angle that calculating the elbow angle is required first and the arm angle has no effect on the elbow joint. It has been described that from the given end-effector pose, the wrist position is calculated first then the elbow joint angle can be obtained to continue the steps of parametrizing the redundancy, therefore, if the elbow joint angle is inside the permissible range, then it possible to calculated and check the limits of the other joint angles otherwise there will be no solutions because the given pose would be outside of the robot workspace.

In the redundancy resolution at the position level using the arm angle parametrization method that has been used in this work, it is possible to avoid the joint limits by obtaining the range of the feasible arm angles for each joint in the manipulator under the given joint limits. From the redundancy circle explained in figure 4-1, it is possible to exclude any arm angle that may command any of the shoulder or wrist joints to exceed its boundary. After eliminating the unfavorable range of the arm angles, then any remaining arm angles will be acceptable to use under the joint limits [33]. As discussed in the previous section that the relation between the arm angle and joint angle can be either monotonic without critical arm angles for the tangent type joints or cyclic with critical arm angle for the tangent and cosine dependence types joints. Each type of the joints profile will be discussed separately because they do not share the same features for calculating the suitable arm angles.

#### 4.4.1 Joint angles without critical arm angles

As discussed in the previous section, the joint angles (1, 3, 5 and 5) with tangent type might not have critical arm angle if the condition in (4.55) is satisfied, meaning that the joint angle at this case increasing or decreasing on some certain arm angle range as shown in figure 4-5 the joint angle will definitely reach to its maximum or minimum as long as the arm angle increase or decrease. Given the upper and lower joint limits, it is possible to calculate the range of the valid arm angles that will always command the corresponding joint angle to stay inside the permissible domain.

Given the upper limit  ${}^n\theta_U$  and lower limit  ${}^n\theta_L$  for joint  $n$  we can calculate the acceptable arm angle range for this type of joint angles from the general form of the tangent type function in (4.45) by the following equations.

$$\psi_{U,L} = \text{atan } 2(a, b) \pm \cos^{-1} \left( \frac{c}{\sqrt{a^2 + b^2}} \right) \quad (4.59)$$

Where a, b and c are given by the following

$$a = X_d \tan({}^n\theta_{U,L}) - X_n$$

$$b = Y_d \tan({}^n\theta_{U,L}) - Y_n$$

$$c = Z_n - Z_d \tan({}^n\theta_{U,L})$$

So the acceptable range of arm angle for this kind of joint angles given by  $[\psi_L, \psi_U]$ . Figure 4-7 illustrates how the suitable arm angles are taken into consideration and the unwanted arm angle are ignored.

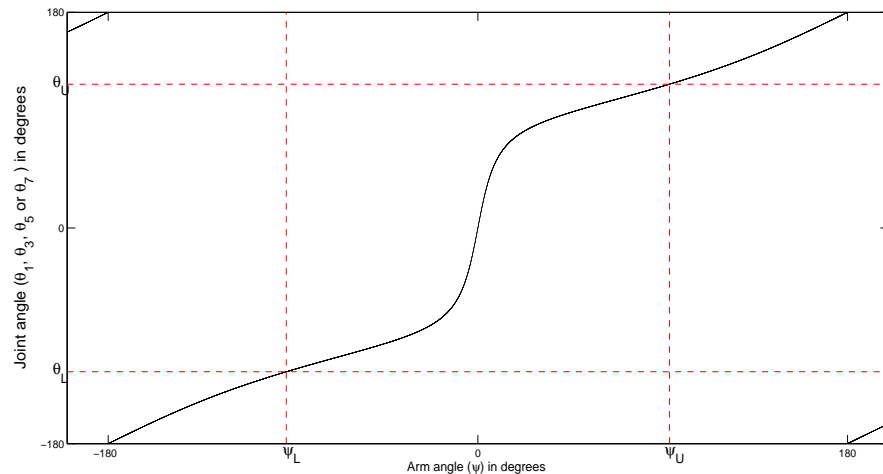


Figure 4-7: The feasible arm angle of the joint angles  $\theta_1, \theta_3, \theta_5$  or  $\theta_7$  when (4.55) is satisfied.

#### 4.4.2 Joint angles with critical arm angles (Cyclic type)

Let us consider the joint angles that have the cyclic profile that have critical arm angles where the joint angles are maximum or minimum as described in the previous section. This kind of the joints behaviour appears whenever the condition in (4.53) is satisfied for the joint 1, 3, 5 and 7. For the joints 2 and 6 there are always critical arm angles so the method of subtracting the unwanted arm angle here is applied to all of the joints with cyclic type.

Let  ${}^n\theta_{max}$  to be the joint angle n value at the maximum arm angle  ${}^n\psi_{max}$  and  ${}^n\theta_{min}$  is the joint angle n value at the minimum arm angle  $\psi_{min}$ . The procedure of calculating the maximum and minimum arm angles for each joint has been described in the previous section. The  ${}^n\theta_U$  and  ${}^n\theta_L$  are the upper and lower limits of the joints respectively. There will be five different cases for calculating the range of the acceptable arm angle for each joint as the following

Case 1:  ${}^n\theta_L \leq {}^n\theta_{max} \leq {}^n\theta_U$  and  ${}^n\theta_L \leq {}^n\theta_{min} \leq {}^n\theta_U$

If the  ${}^n\theta_{max}$  and  ${}^n\theta_{min}$  are between the upper and lower limits, then there is no need to exclude any arm angle for this joint. As shown in figure 4-8 whatever the value of the arm angle is, the joint angle is still within the allowable range.

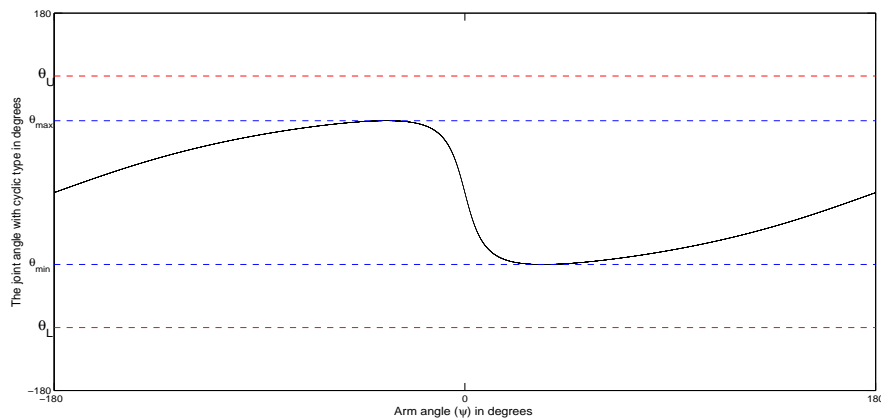


Figure 4-8: Case 1: The full range of the arm angle is acceptable.

Case 2:  ${}^n\theta_L \leq {}^n\theta_{min} \leq {}^n\theta_U$  and  ${}^n\theta_{max} > {}^n\theta_U$

If the  ${}^n\theta_{min}$  is between the upper and lower limits, and the  ${}^n\theta_{max}$  is greater than the upper limit of the joint as shown in figure 4-9, then there is a need to exclude the range of the arm angles that make the joint angle greater than allowable. The boundaries of the range can be calculated by the following equation

$$\psi_{U,L} = \text{atan} 2(a, b) \pm \cos^{-1} \left( \frac{c}{\sqrt{a^2 + b^2}} \right) \quad (4.60)$$

Where a, b and c are given by

$$a = X_d \tan({}^n\theta_U) - X_n$$

$$b = Y_d \tan({}^n\theta_U) - Y_n$$

$$c = Z_n - Z_d \tan({}^n\theta_U)$$

The values  $X_n, Y_n, Z_n, X_d, Y_d, Z_d$  are the constants calculated from the given position and orientation of the end-effector (see section 4.2). Assuming that the elbow is rotating around the shoulder-wrist axis starting from  $-180^\circ$  to  $180^\circ$  as the example in figure 4-9, then the acceptable range is the union of the two intervals  $[-180, \psi_1]^\circ$  and  $[\psi_2, 180]^\circ$ . The arm angle range  $[\psi_1, \psi_2]^\circ$  must be excluded.

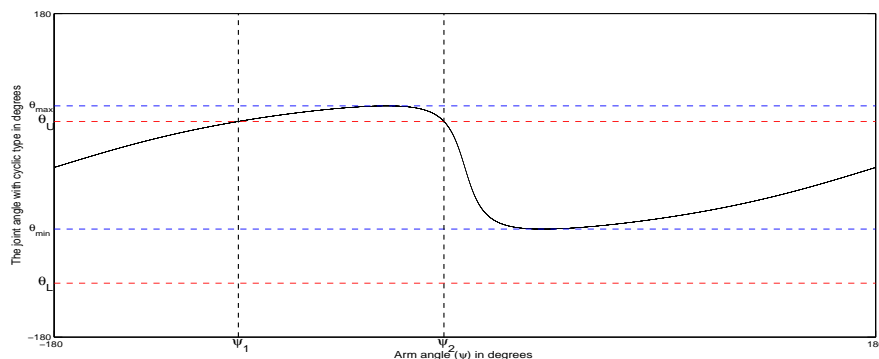


Figure 4-9: Excluding the arm angle range when the maximum joint angle is greater than the upper limit.

Case 3:  ${}^n\theta_L \leq {}^n\theta_{max} \leq {}^n\theta_U$  and  ${}^n\theta_{min} < {}^n\theta_L$

If the  ${}^n\theta_{max}$  is between the upper and lower limits, and the  ${}^n\theta_{min}$  is less than the lower limit of the joint as shown in figure 4-10, then there is a necessity to eliminate the range of the arm angles that make the joint angles less than permissible. The boundaries of the arm angle range can be calculated by equation (4.60) where a, b and c are given by the following:

$$a = X_d \tan({}^n\theta_L) - X_n$$

$$b = Y_d \tan({}^n\theta_L) - Y_n$$

$$c = Z_n - Z_d \tan({}^n\theta_L)$$

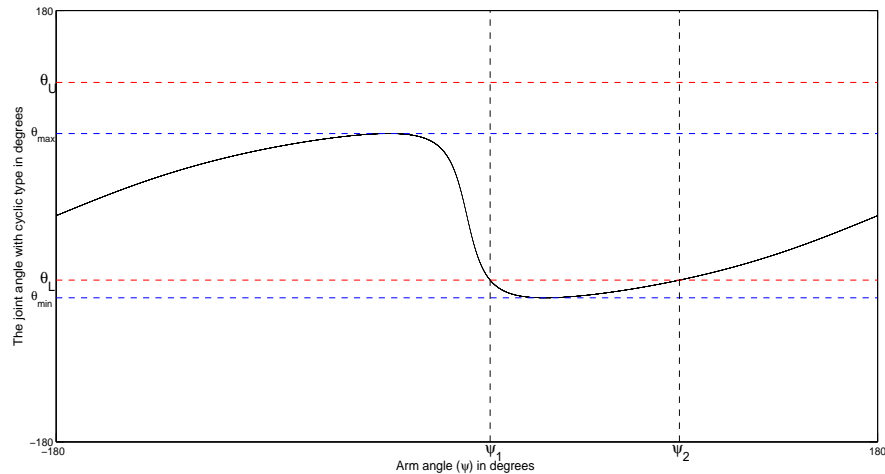


Figure 4-10: Excluding the arm angle range when the minimum joint angle is less than the lower limit.

Case 4:  ${}^n\theta_{max} > {}^n\theta_U$  and  ${}^n\theta_{min} < {}^n\theta_L$

If the joint angle  ${}^n\theta_{max}$  at the maximum arm angle is greater than the upper limits and the joint angle  ${}^n\theta_{min}$  at the minimum arm angle is less than the lower limit of the joint as shown in figure 4-11, then we need to exclude two domains from the full cycle of the arm angles. The boundaries of the range can be calculated by equation (4.60) where a, b and c are used once in the form of case 2 to eliminate the range between  $[\psi_1, \psi_2]$  and another time as the forms of case 3 to eliminate the range between  $[\psi_3, \psi_4]$ . Choosing any value for the arm angle other than these two ranges would command the joint to stay at the allowable range.

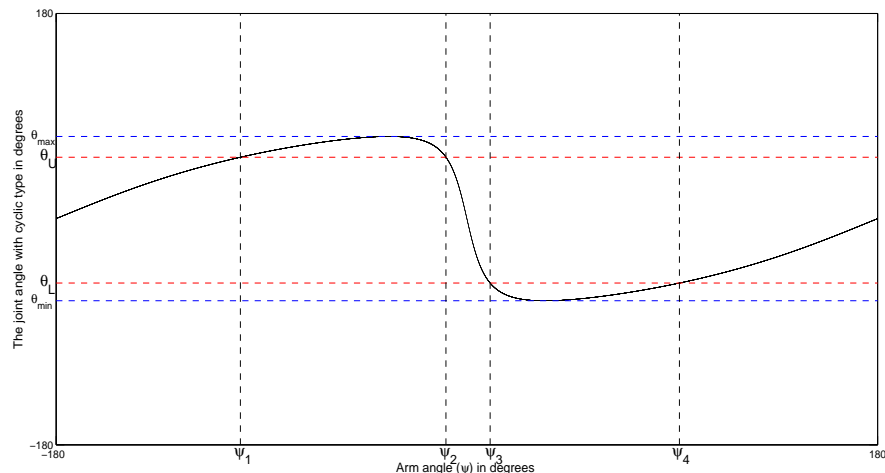
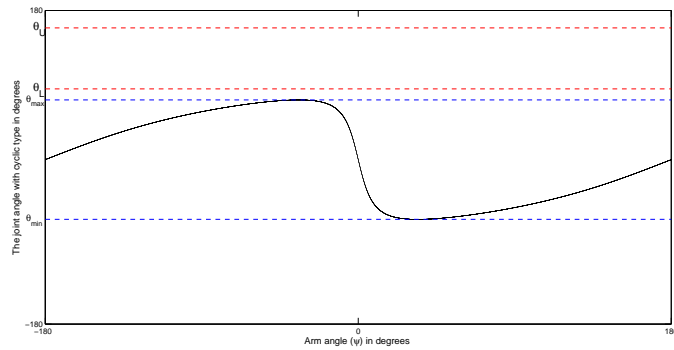


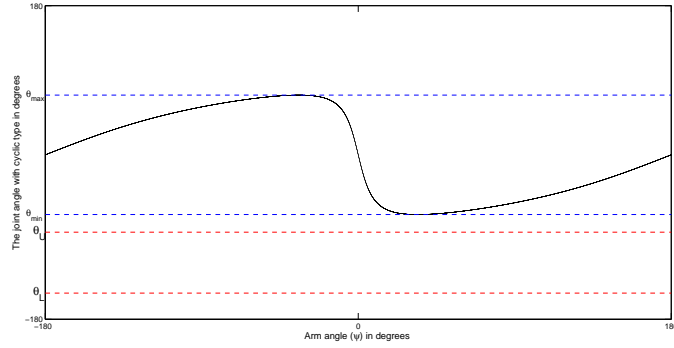
Figure 4-11: Two arm angle domains to be eliminated.

Case 5:  ${}^n\theta_{max} < {}^n\theta_L$  or  ${}^n\theta_{min} > {}^n\theta_U$

If the  ${}^n\theta_{max}$  is less than the lower limits, or the  ${}^n\theta_{min}$  is greater than the upper limit of the joint as shown in figure 4-12, then the entire domain of the arm angle is not available and no solution can be obtained. Meaning that the given pose of the end-effector is outside the workspace of the manipulator [4]. After calculating the



(a)



(b)

Figure 4-12: The entire domain of the arm angle is not acceptable:(a) when  $\theta_{max} < \theta_L$   
(b):  $\theta_{min} > \theta_U$ .

acceptable ranges of the arm angle for each joint in the manipulator, the intersection of these domains will be taken at final as the acceptable domain because the selected arm angle must be accepted by all the joints simultaneously.

## 4.5 Singularity configurations and avoidance

In the robot manipulators, the singularity configurations may occur when the number of the degrees of freedom of the arm are less than the number of the task space elements that are describing the end-effector posture, i.e. the location of the tool center point and the orientation of the tool. One of the advantages of redundant manipulators is making use of the redundancy to avoiding the singularity configurations. As mentioned before the redundant manipulators generate infinitely many joint trajectories, so it possible to make use of the redundancy to avoid choosing any joint trajectory that may lead to discontinuity. Another kind of singularities are called algorithmic singularities, which may appear due to a particular method developed to perform additional tasks such as avoiding the joint limits [16].

### 4.5.1 Kinematic singularities

For 7-DOF kinematic robot with S-R-S type as the robot arm model in this study, there are three kinematic singularities which are the elbow, shoulder and wrist singularities [6]. The elbow singularity is called the external singularity while the shoulder and wrist singularities are called the internal singularities. The elbow singularity occurs when the arm reaches a boundary of the workspace that happens when the manipulator is fully extended as shown in figure 4-13. This kind of singularity can not be avoided because there is always maximum reach of the arm at the boundaries in the workspace [34]. The shoulder and wrist singularities are called internal singularities because this kind of singularities are occur inside the boundaries of the workspace. Theses singularities can be avoided by using the self-motion of the arm by avoiding choosing any arm angle, which may push any of the joint angles into the singularity configuration [35].

The shoulder singular configuration appears in one case when the wrist position stretch on the same line of joint 1 axis [34] as shown in figure (4-14). It means that the x and y components of the wrist position at this case are zeros. This will lead

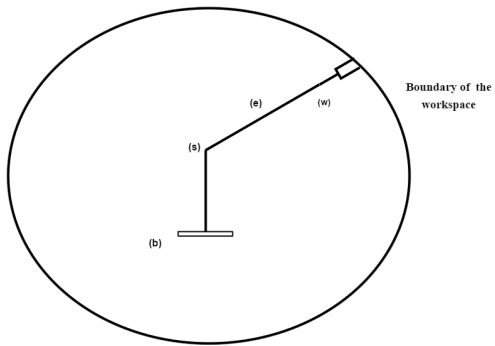


Figure 4-13: Elbow singularity configuration.

the reference joint angle  $\theta_1'$  given by equation (4.11) to be undetermined. It can be realized that in this singularity from the definition of the arm angle the joint 1 and the arm angle are equal. [32] claimed that by making the joint angle 1 equal to zero the problem will be solved in this case. The wrist singularity happened when the wrist is in line, this singularity is always avoidable by using the arm angle of the manipulator to reconfigure the arm to make the wrist not straight [6].

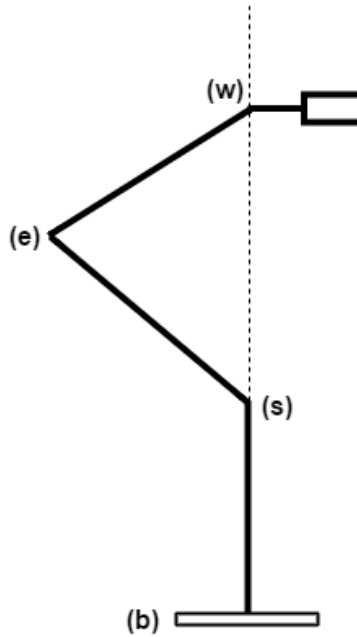


Figure 4-14: Shoulder singularity configuration.

### 4.5.2 Algorithmic Singularities

From the tangent type of joint angles given by equations (4.25), (4.30), (4.40) and (4.44) it can be verified that if the numerator and denominator in these equations are zero, then the joint angles are indeterminate, meaning that (4.61) is satisfied. In this case the singular arm angle can be calculated as shown in (4.62). It is possible to study the profile of the joints around the singular arm angle using the limit analysis. Avoiding the discontinuity can be achieved by not selecting the singular arm angle because all the joint angles can be determined except at the singular arm angle. It can be realized that the redundancy parametrization method discussed previously can solve this problem effectively.

$$x^2 + y^2 - z^2 = 0 \quad (4.61)$$

The singular arm angle need to be avoided is

$$\psi_t = 2 \tan^{-1} \left( \frac{x}{y - z} \right) \quad (4.62)$$

For the cosine joint angles (2 and 6) type the algorithmic singularity occur if  $\sin(\theta)$  in equation (4.57) is equal to zero. In order to avoid this singularity we can calculate the arm angles which lead to this singularity. It is known that if  $\theta=0$  or  $\pi$  then  $\sin(\theta)$  will be zero.

Substituting  $\theta=0$  into (4.56), the arm angle in this case is as the following :

$$\psi_{cs1} = 2 \tan^{-1} \left( \frac{x_c}{y_c - z_c + 1} \right) \quad (4.63)$$

Similarly  $\theta=\pi$  into (4.56), the singular arm angle in this case is as the following :

$$\psi_{cs2} = 2 \tan^{-1} \left( \frac{x_c}{y_c - z_c - 1} \right) \quad (4.64)$$

# Chapter 5

## Results and Analysis

This chapter presents the algorithms summary of the inverse kinematic problem by computing the joint angles in term of the redundancy parameter and the algorithms of forbidding any arm angle that lead any of the joint angles to exceed allowed limits. After that the robot workspace of the 7-DOF manipulator studied in this chapter. The methods discussed in chapter 4 is examined to show the redundant joint motion while the end-effector is stationary at a specific pose. An example is presented to validate how to make use of the redundancy circle to avoid the joint limit constraints. The last section shows some examples on how this method can be used to follow a straight line trajectory with high accuracy and low computation cost by initiating a motion as sequence of points between initial and final pose like up and down motions, movements right-left and forward-backward motions. As mentioned before that the inverse kinematic problem in this work was solved at the position level where the redundancy must be represented by a parameter  $\psi$ . Algorithm 1 summaries the method of calculating the joint angles in term of the arm angle. Algorithm 2 concludes the method of how to select a proper arm angle  $\psi$  to avoid the joint angle limits as a secondary task requirement for any given pose inside the robot workspace.

## 5.1 Algorithm summary

The first algorithm solves the inverse kinematics problems in an analytical form parametrized by the arm angle  $\psi$  under no additional restrictions.

---

**Algorithm 1** Inverse kinematics

---

```
1: procedure JOINT ANGLES COMPUTATION IN TERM (ARM ANGLE  $\psi$ )
2:   for each given position and orientation of the end-effector do
3:     Compute the wrist position relative to the base  $w$  using equation (4.1)
4:     Compute the wrist position relative to the shoulder  ${}^sL_w$  using (4.2)
5:     Compute the length (norm) of the vector connecting the wrist and the
       shoulder  $|{}^sL_w|$  obtained in step 4
6:     Calculate the joint 4 angle,  $\theta_4$ , using equations (4.9) and (4.10)
7:     if  $\theta_4$  exceeds the joint 4 upper and lower limits then
8:       The given pose is outside the robot workspace
9:     else
10:      Compute the skew symmetric matrix  ${}^s k_w$  using (4.5)
11:      Compute the Rodrigues formula representing the rotating vector  ${}^s L_w$ 
        with the arm angle  $\psi$  using equation (4.4)
12:      Set  $\theta_3$  to zero and calculate the reference joint angles  $\theta'_1$  and  $\theta'_2$  of the
        reference plane using equations (4.11) and (4.12) respectively
13:      Calculate the rotation matrix of the reference joint angles using (4.16)
14:      Compute the shoulder constant matrices  $X_s$ ,  $Y_s$  and  $Z_s$  by (4.20)-(4.22)
15:      Compute the shoulder joint angles  $\theta_1$ ,  $\theta_2$  and  $\theta_3$  in term of arm angle
         $\psi$  using equations (4.26), (4.28) and (4.30) respectively
16:      Compute the wrist matrices  $X_w$ ,  $Y_w$  and  $Z_w$  by (4.34)-(4.36)
17:      Compute the wrist joint angles  $\theta_5$ ,  $\theta_6$  and  $\theta_7$  in term of arm angle  $\psi$ 
        using equation (4.40), (4.42) and (4.44) respectively
18:    end if
19:  end for
20: end procedure
```

---

The second algorithm gives a set of values of the arm angle parameter in the form of a union of intervals. If this set is not empty, every value from it can be used to find a particular solution of the inverse kinematics problem that is consistent with the given restrictions on the values of the joint variables.

---

**Algorithm 2** Automatic method to choose a suitable arm angle

---

```

1: procedure FEASIBLE ARM ANGLE  $\psi$  UNDER JOINT LIMIT
2:   for each given position and orientation of the tool do
3:     Compute the wrist position relative to the base  $w$  using equation (4.1)
4:     Compute the wrist position relative to the shoulder  ${}^sL_w$  using (4.2)
5:     Compute the length (norm) of the vector connecting the wrist and the
       shoulder  $|{}^sL_w|$  calculated in step 4
6:     Calculate the joint 4 angle  $\theta_4$  using equations (4.9) and (4.10)
7:     if  $\theta_4$  exceeds the joint 4 upper and lower limits then
8:       The given position and orientation are outside the robot workspace
9:     else
10:      Compute the skew symmetric matrix  ${}^s k_w$  of the vector between the
        wrist and the shoulder using equation (4.5)
11:      Set  $\theta_3$  to zero and calculate the reference joint angles  $\theta'_1$  and  $\theta'_2$  of the
        reference plane using equations (4.11) and (4.12) respectively
12:      Calculate the rotation matrix of the reference joint angles using
        equation (4.16)
13:      Compute the shoulder constant matrices  $X_s$ ,  $Y_s$  and  $Z_s$  that relate the
        shoulder joint angles to the arm angle using equations (4.20)-(4.22)
14:      Compute the wrist constant matrices  $X_w$ ,  $Y_w$  and  $Z_w$  that relate the
        wrist joint angles to the arm angle using equations (4.34)-(4.36)

```

---

---

```

15:   for each tan joint type (1, 3, 5 and 7) do
16:     Calculate the coefficients x, y and z using equations (4.48), (4.49)
        and (4.50) respectively
17:     if equation (4.53) is satisfied then
18:       The joint angle type with respect to the arm angle is cyclic
19:       Calculate the critical arm angles using equations (4.51) and
        (4.52) and check which one of them gives maximum joint angle
         $\theta_{max}$  and which one gives the minimum joint angle  $\theta_{min}$  using
        equation (4.54)
20:       If the maximum and minimum joint angles are between the upper
        and lower limits, then any arm angle can be chosen for that joint
21:       If the maximum joint angle is greater than the upper limit and
        the minimum joint angle is between the upper and lower limits,
        then the feasible arm angle can be calculated using equation
        (4.60)
22:       If the minimum joint angle is less than the lower limit and the
        maximum joint angle is between the upper and lower limits, then
        the feasible arm angle can be calculated using equation (4.60)
        with a, b and c coefficients given on page 57
23:       If the minimum joint angle is less than the lower limit and the
        maximum joint angle is greater than the upper limit, then the
        feasible arm angle can be calculated using equation (4.60) with
        a, b and c coefficients given on pages 56 and 57
24:       If the minimum joint angle is greater than the upper limit or
        the maximum joint angle is less than the lower limit, then there
        is no feasible arm angle
25:     end if
26:     if equation (4.53) is not satisfied then
27:       The tan type joint angle is monotonic. The suitable arm angle
        range can be calculated using equation (4.59)
28:     end if
29:   end for
30:   for each cos joint type (2 and 6) do
31:     All cos type joints are cyclic
32:     Find the critical angle  $\psi_c$  using equation (4.58)
33:     Find the other critical angles which are  $\psi_c \pm \pi$ 
34:     Use the first derivative in equation (4.57) to check which one is the
        maximum and which one is the minimum arm angle
35:     Find the maximum and minimum joint angle for each cos type joint
36:     Repeat the steps from 20 to 25 to find the suitable arm angle ranges
37:   end for
38:   Find the intersection of all the arm angle ranges of all joints which will
        be feasible to all joints
39:   end if
40: end for
41: end procedure

```

---

## 5.2 Robot workspace

The workspace of the robot is the set of all possible positions that can be reached by the end-effector. It gives a better picture of the robot's working environment. The D-H method used to derive the forward kinematics presented in chapter 2 will be used to generate the robot workspace by calculating the position of the end-effector. An approximate workspace will be generated in this work using Monte Carlo method, which is a random sampling numerical method that can be applied to the joint space of the manipulator [36][37]. This method avoids the complexity of analytical derivation of the robot workspace. The method works as randomly choosing some values for each joint then calculating the end-effector position using the proposed forward kinematics D-H methods. Let's assume  $i$  samples generated for each joint angle  $n$  between its lower and upper limits using the following equation

$$\theta_{ni} = \theta_{Ln} + (\theta_{Un} - \theta_{Ln})rand(i, 1) \quad (5.1)$$

Where  $n$  is number of the joint,  $\theta_{Ln}$  and  $\theta_{Un}$  are the lower and upper limits of the joint  $n$  and  $rand(i, 1)$  is a result of using the corresponding Matlab function that generates random number between zero and one. The upper and lower limit values used to plot the workspace in this work were taken from the technical data of the Dextrous Lightweight Arm (LWA 4D) available at Schunk company website. Table 5.1 presents the joint angle limits.

Table 5.1: The lower and upper limits of each joint

Joint $n$	1	2	3	4	5	6	7
${}^n\theta_U$ (deg)	180	123	180	125	180	170	170
${}^n\theta_L$ (deg)	-180	-123	-180	-125	-180	-170	-170

The number of random sample values  $i$  generated to plot the workspace shown in figure 5.1 are 50000. Increasing the value of  $i$  gives always better results and good picture of the robot workspace. Figure 5-1 shows the robot workspace in 3 dimensional view as a roughly ellipsoid. The figure also illustrates the robot workspace projection in XY plane, the movement range between [-0.7334,0.7334]m in X-axis, the robot workspace projection in YZ plane shows that the robot can move along Y-axis between [-0.7334,0.7334]m while the range along z-axis is [-0.26,1.0334]m.

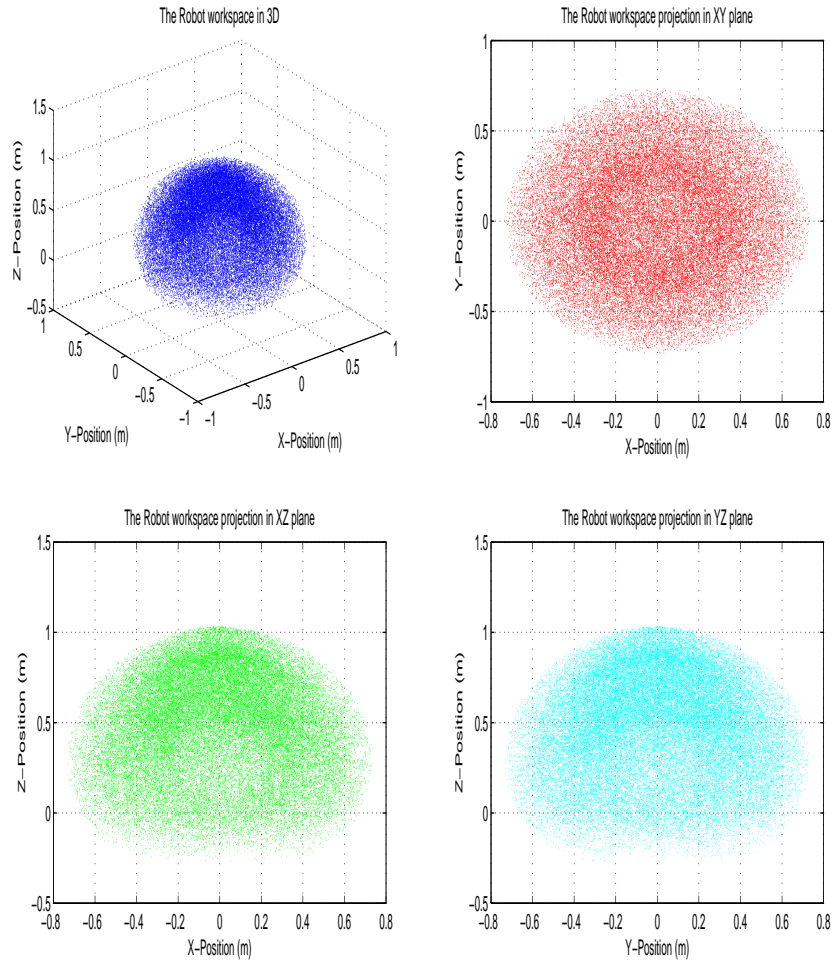


Figure 5-1: The robot workspace.

### 5.3 The redundancy circle at a stationary end-effector

This section describes the self-motion of the robot manipulator while the end-effector is fixed at a specific pose in the absence of any restrictions such as joint limits to verify the methods discussed in chapter 4, the next section will consider the joint limits constraint. As mentioned before that the redundancy circle in this arm appears when the elbow rotate around the axis between the shoulder and the wrist. Varying the arm angle keeping specific stationary end-effector posture shows the self motion in the arm. Let us consider rotating the elbow of the manipulator two full rotation around the line connecting the shoulder and wrist where  $\Psi \in [-360,360]^\circ$  to have a better idea on the joints variation when the redundancy parameter changes. Let's assume that the end-effector is fixed at the following pose

$$T = \begin{bmatrix} 1 & 0 & 0 & -0.0030 \\ 0 & 1 & 0 & 0.3000 \\ 0 & 0 & 1 & 0.5000 \\ 0 & 0 & 0 & 1.0000 \end{bmatrix} \quad (5.2)$$

Figure 5-2 shows the seven joint profiles versus the redundancy parameter ( $\psi$ ). The joint angles  $\theta_1$  and  $\theta_7$  are tan type functions as shown in equations (4.26) and (4.44). The tan type joint angle may have cyclic behaviour with maximum and minimum joint angles at the critical arm angles or it might be continuously increasing or decreasing on a certain arm angle range with no critical arm angles. In this example equation (4.50) is satisfied for the joints  $\theta_1$  and  $\theta_7$  at this pose so profiles of these joints have cyclic manner. It shows that each of them have same behaviour on the interval  $[-360,0]^\circ$  and  $[0,360]^\circ$  and they will continue to do so for  $\Psi \in [\theta, \theta + 360]^\circ$ . The joint angles  $\theta_2$  and  $\theta_6$  are cos type functions as shown in equations (4.28) and (4.42) respectively. The cos type joint angle has always cyclic behaviour with maximum and minimum joint angles at the critical arm angles. The critical arm angle can be calculated using equation (4.58). The joints style shows that in every full

rotation of the elbow around shoulder-wrist axis that the critical arm angles are  $180^\circ$  apart from each other. It illustrates as well that these joints have same behaviour on consequences intervals as shown on  $[-360,0]^\circ$  and  $[0,360]^\circ$  and it will have the same profile for  $\Psi \in [\theta, \theta+360]^\circ$ .

The joint angles  $\theta_3$  and  $\theta_5$  are tan type functions as shown in equations (4.30) and (4.40). Even though these joints are tan type functions like joint 1 and joint 7 but they are not cyclic. The results shows that the angles are continuously increasing in joint 3 and decreasing in joint 5 on a certain arm angle range with no critical arm angles. This happens because equation (4.53) is not satisfied for these joints at the specified pose. It shows that these joints have same behaviour on the interval  $[-360,0]^\circ$  and  $[0,360]^\circ$  and it will continue so for  $\Psi \in [\theta, \theta+360]^\circ$ . It's also worth to note that joint 3 makes a full rotation when the arm angle parameter is at  $-180^\circ$  and  $180^\circ$  while the joint angle 5 makes a full rotation at  $-360^\circ$ ,  $0^\circ$  and  $360^\circ$ .

Joint angle 4 is constant as shown in the figure because it does not depend on the arm angle.

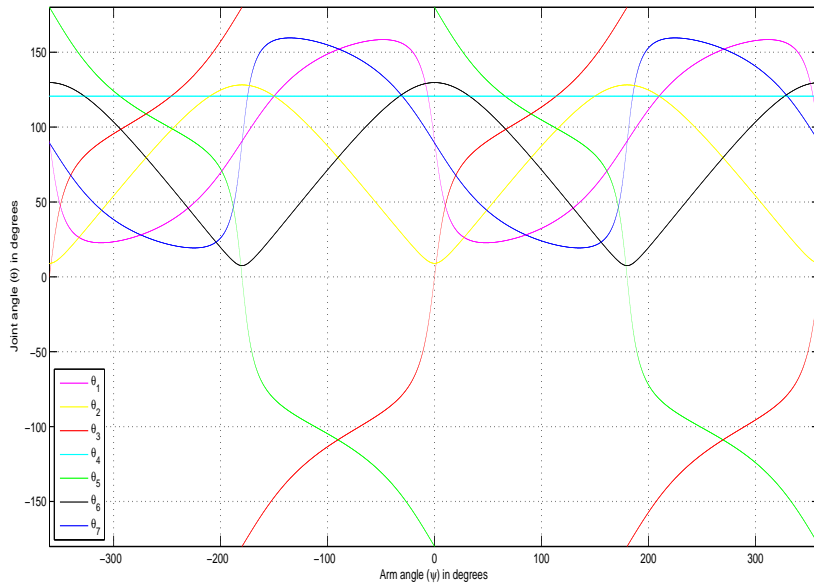


Figure 5-2: The joints curves with respect to the arm angle at pose in (5.2).

The joint angles  $\theta(\psi^\circ)$  in figure 5-2 are the same at  $\theta(-360^\circ)$ ,  $\theta(0^\circ)$  and  $\theta(360^\circ)$

where

$$\theta_1=90.5729^\circ, \theta_2=9.0346^\circ, \theta_3=0^\circ, \theta_5=180^\circ, \theta_6=129.7020^\circ \text{ and } \theta_7=89.4271^\circ$$

These joints are always the same at any  $\psi$  and  $\psi+360^\circ$ .

Figure 5-3 illustrates the redundancy circle (elbow movement) at the stationary end-effector in (5.2) and its projections at XY, XZ and YZ planes. It shows that the elbow move in a circular form around axis connecting the shoulder and wrist.

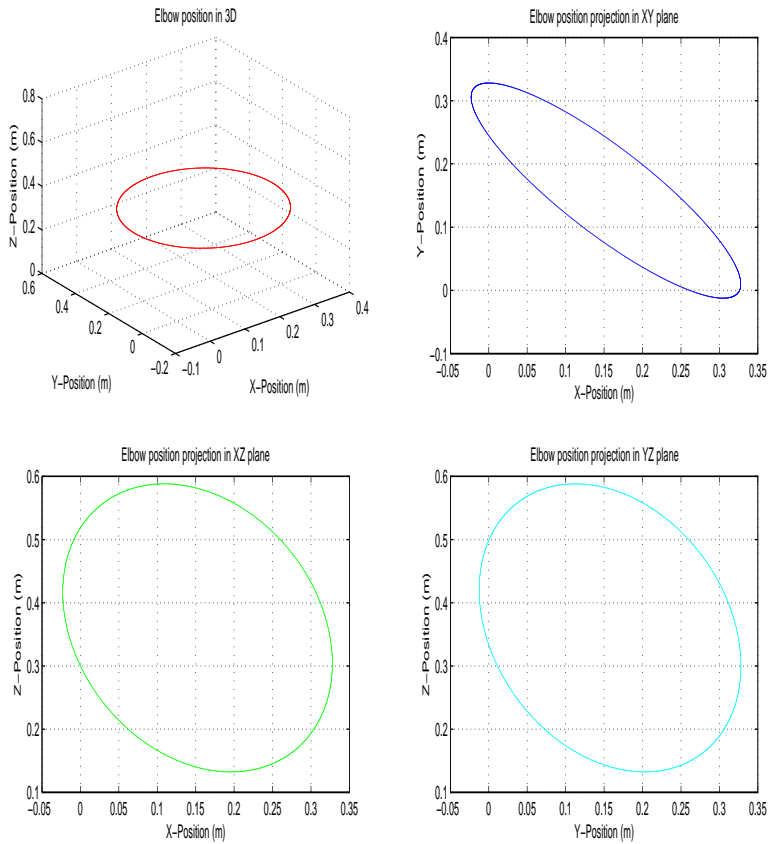


Figure 5-3: Redundancy circle at the pose in (5.2).

## 5.4 Redundancy resolution under joint limits

This section presents some tests on how the methods discussed in chapter 4 can be used to avoid the joint limits by choosing a suitable arm angle that forces the joints to stay at the permissible range for each joint. As mentioned before, the redundancy parameter, which does not exceed the limits of the joints can be calculated from the given position and orientation of the end-effector. The method takes the pose of the tool and finds the suitable arm angle range then calculates the joint angles as shown in figure 5-4.

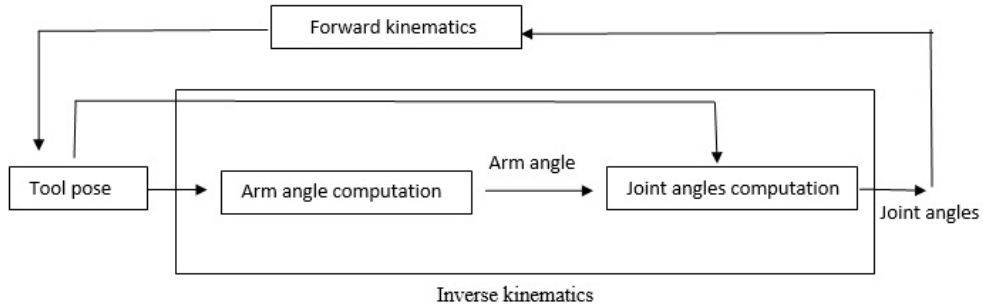


Figure 5-4: Forward and inverse kinematics block diagram.

Let's assume that the pose of the end-effector is as shown in (5.3).

$$P = \begin{bmatrix} 1.0000 & 0.9211 & 0.3894 & 0.3000 \\ 0 & -0.9211 & -0.3894 & -0.3000 \\ 1.0000 & 0.3894 & -0.9211 & 0.4000 \\ 0 & 0 & 0 & 1.0000 \end{bmatrix} \quad (5.3)$$

Each joint will be studied separately to clarify the idea on how to choose the suitable arm angles range and ignore the range which leads the joint angle to violate its limits. Joint angle 4 (elbow joint) will not be studied here because it does not depend on the arm angle, meaning that choosing any arm angle would not change the value of joint 4 angle.

Figure 5-5 shows how each joint react with varying the arm angle between [-180,180]

degrees as one full rotation of the elbow around the shoulder-wrist axis. I will assume new smaller joint limits in this example as in table 5.2 to have a better idea on how redundancy can be resolved under joint limits.

Table 5.2: Assumed stricter upper and lower limits

Joint $n$	1	2	3	4	5	6	7
${}^n\theta_U(\text{deg})$	150	100	120	125	150	100	130
${}^n\theta_L(\text{deg})$	-150	-100	-120	-125	-150	50	-130

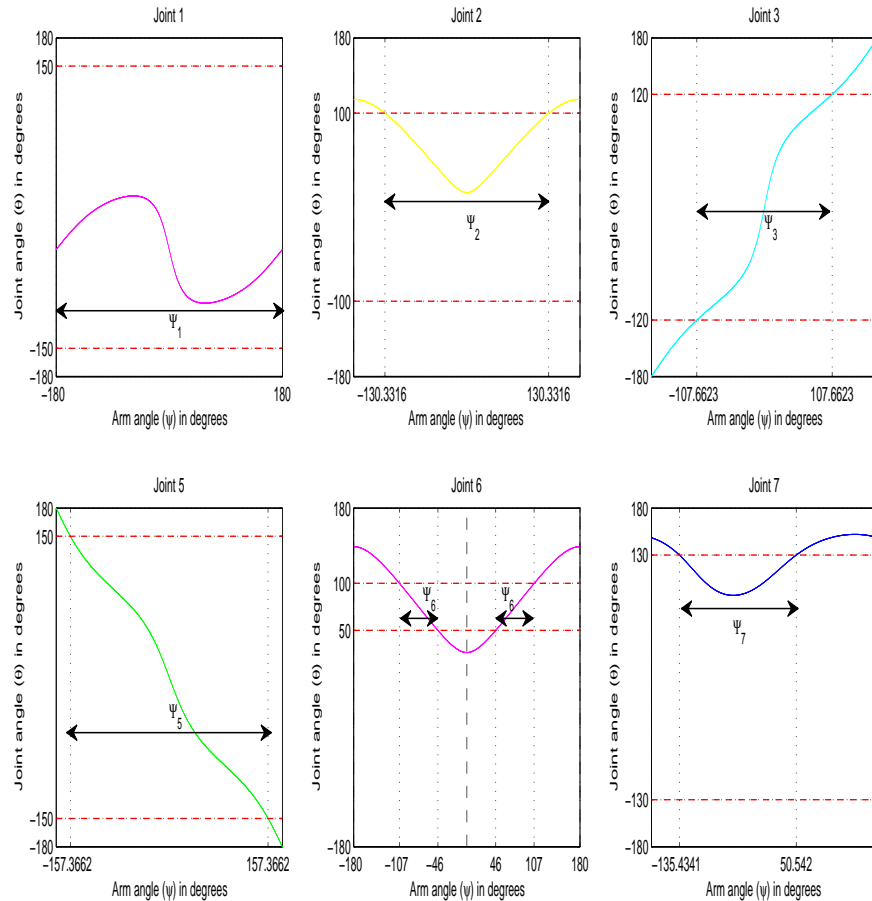


Figure 5-5: Joint angles versus the arm angle at pose in (5.3).

**Joint angle ( $\theta_1$ ):** Joint angle  $\theta_1$  is a tan type function as shown in equation (4.26). As mentioned before, the tan type joint angle may have cyclic behaviour with maximum and minimum joint angles at the critical arm angles or it might be continuously increasing or decreasing on a certain arm angle range with no critical arm angles. Equation (4.53) is satisfied at this pose where  $x^2 + y^2 - z^2 = 0.1410 > 0$  meaning that the joint angle 1 is cyclic as shown in figure 5-5, the two critical arm angles are  $56.9921^\circ$  and  $-56.9921^\circ$  which are calculated using equations (4.51) and (4.52). The joint angle is minimum at one of them and maximum at the other one. The second derivative equation (4.54) at  $\psi=56.9921^\circ$  is positive and negative at  $\psi=-56.9921^\circ$  so the maximum joint angle obtained is  $\theta_{max}=12.0436^\circ$  and the minimum joint angle is  $\theta_{min}=-102.0438^\circ$ . Both the maximum and minimum joint angles are between the upper and lower limits. This shows that choosing any arm angle will not lead joint 1 to exceed its limits where the feasible arm angle for joint 1 is  $\Psi_1=[-180,180]^\circ$ .

**Joint angle ( $\theta_2$ ):** The joint angle  $\theta_2$  is a cos type function as shown in equation (4.28). As mentioned before, the cos type joint angle conduct with respect to the arm angle is always cyclic having maximum and minimum joint angles at the critical arm angles as joint angle 2 shows in figure 5-5. The critical arm angle calculated using equation (4.58) which is  $\psi_c=0^\circ$ . The other critical arm angle is  $\psi_c=\pm 180^\circ$ . Using the first derivative function in (4.57), the results found that the joint angle  $\theta_2$  is minimum at  $\psi_c=0^\circ$  and maximum at  $\psi_c=\pm 180^\circ$  so the maximum joint angle obtained is  $\theta_{max}=114.6546^\circ$  and the minimum joint angle is  $\theta_{min}=15.5443^\circ$ . The results shows that minimum joint angle is in between the upper and lower limits while the maximum joint angle exceed the upper limits of the second joint  $\theta_U=100^\circ$ . For this reason some values of the arm angle must be excluded by substituting the upper limits of joint 2 into equation (4.60). The results obtained show that the joint angle stay at its permissible limits when the arm angle inside  $\Psi_2 \approx [-130.3316, 130.3316]^\circ$ .

**Joint angle ( $\theta_3$ ):** Joint angle  $\theta_3$  is a tan type function as shown in equation (4.30) similar to the joint angle  $\theta_1$  but this joint has no critical arm angles because equation (4.53) is not satisfied at this pose where  $x^2 + y^2 - z^2 = -0.2003$  which is  $< 0$  meaning that this joint angle will be monotonically increasing or decreasing on a certain arm angle range. This joint angle is monotonically increasing because the first derivative of this joint is always positive at any arm angle as shown in figure5-5. The correspondent range of arm angles to the upper and lower limit of joint 5 is  $\Psi_3 \approx [-107.6623, 107.6623]^\circ$ .

**Joint angle ( $\theta_5$ ):** Joint angle  $\theta_5$  is a tan type function as well as shown in equation (4.40). This joint angle is also monotonic because equation (4.53) is not satisfied at this pose. Unlike joint angle 3, the joint  $\theta_5$  is monotonically decreasing because the first derivative of this joint is always negative at any arm angle as shown in figure5-5. The correspondent interval of arm angles to the upper and lower limit of joint 5 is  $\Psi_5 \approx [-157.3662, 157.3662]^\circ$ .

**Joint angle ( $\theta_6$ ):** The joint angle  $\theta_6$  is a cos type function as shown in equation (4.42). It has the same manner as joint angle 2, see figure 5-5. There is critical arm angle calculated using equation (4.58) which is  $\psi_c=0^\circ$ . The other critical arm angle is  $\psi_c=\pm 180^\circ$ . Using the first derivative function in (4.57), the results obtained that the joint angle  $\theta_6$  is minimum at  $\psi_c=0^\circ$  and maximum at  $\psi_c=\pm 180^\circ$ . The maximum joint angle is  $\theta_{max}=138.9365^\circ$  and the minimum joint angle is  $\theta_{min}=26.3962^\circ$ . The results shows that minimum joint angle is less than the lower limits which is  $\theta_L=50^\circ$  and the maximum joint angle is greater than the upper limits of this joint which is  $\theta_U=100^\circ$ . Based on the max and min joint angle results, some values of the arm angle must be discarded by substituting the upper and lower limits of joint 6 into equation (4.60). The results obtained are that the joint angle stay at its permissible limits when the arm angle belongs to  $\Psi_6 \approx [-107.2425, -46.1061] \cup [46.1061, 107.2425]^\circ$  as shown on figure 5-5.

**Joint angle ( $\theta_7$ ):** As shown in equation (4.44), joint angle  $\theta_7$  is a tan type function. This joint angle is a cyclic with maximum and minimum joint angles at the critical arm angles as shown in figure 5-5. At this pose, equation (4.53) is satisfied where  $x^2 + y^2 - z^2 = 0.4647 > 0$ , the two critical arm angle are  $-49.7041^\circ$  and  $144.0932^\circ$  that are computed using equations (4.51) and (4.52). The maximum joint angle that can be reached is  $\theta_{max} = 152.0057^\circ$  at the critical arm angle  $\psi = 144.0932^\circ$  and the minimum joint angle is  $\theta_{min} = 87.1641^\circ$  at the critical arm angle  $\psi = -49.7041^\circ$ . The minimum joint angle is between the lower and upper limits of joint 7 while it exceeds the upper limits at some arm angle range which needs to be discarded. Substituting the upper limit of joint 7 into equation (4.60), the result obtained that the suitable arm angle range for this joint is  $\Psi_7 \approx [-135.4341, 50.5420]^\circ$ .

So after subtracting all the forbidden intervals from the redundancy circle we obtain

$$\Psi_1 = [-180, 180]^\circ$$

$$\Psi_2 \approx [-130.3316, 130.3316]^\circ$$

$$\Psi_3 \approx [-107.6623, 107.6623]^\circ$$

$$\Psi_5 \approx [-157.3662, 157.3662]^\circ$$

$$\Psi_6 \approx [-107.2425, -46.1061]^\circ \cup [46.1061, 107.2425]^\circ$$

$$\Psi_7 \approx [-135.4341, 50.5420]^\circ$$

and the overall feasible arm angle is  $\Psi \approx [-107.2425, -46.1061]^\circ \cup [46.1061, 50.5420]^\circ$ . Choosing any arm angle from these intervals would force the joint angles to be inside the allowable range for all of them. Lets assume that the middle value of the first feasible interval is chosen where  $\psi = -76.6732^\circ$ . This arm angle would give the following joint angles

$$\theta_1 = 10.2132^\circ$$

$$\theta_2 = 64.3891^\circ$$

$$\theta_3 = -101.8298^\circ$$

$$\theta_4 = 100.1720^\circ$$

$$\theta_5 = 86.1546^\circ$$

$$\theta_6 = 74.8701^\circ$$

$$\theta_7 = 92.1828^\circ$$

The obtained results shows that all the joint angles are inside the joints allowable ranges. Let's select the maximum allowable arm angle  $\psi=50.5420^\circ$ . The joint angles at this arm angle are as the following

$$\theta_1 = -101.7902^\circ$$

$$\theta_2 = 44.6139^\circ$$

$$\theta_3 = 85.6369^\circ$$

$$\theta_4 = 100.1720^\circ$$

$$\theta_5 = -67.3344^\circ$$

$$\theta_6 = 53.4793^\circ$$

$$\theta_7 = 129.9993^\circ$$

The results showing that all the joints are between their limits and joint 7 shows that it is almost approaching its limits, choosing any greater arm angle would lead joint 7 to violate its limits.

## 5.5 Straight line Cartesian trajectories

This section presents examples of following straight line trajectories using inverse kinematics as a standard method used to control the robot arms by finding the correspondent joint angles at the joint space for a planned trajectory at the Cartesian space. As mentioned before the redundant manipulators can generate infinitely many joint trajectories at the joint space that lead to the same planned trajectory at the task space. Some of these joint trajectories must be eliminated to meet other secondary requirements such as avoiding the joint limits. As discussed before the inverse kinematics and redundancy resolution in this work was solved at the position level to allow better accuracy than achievable with resolutions on the velocity level. A point-to-point trajectories are planned along straight lines on the X-axis, Y-axis and Z-axis. The trajectory is discretized between two defined poses and at each position and orientation, the redundancy is resolved to find range of suitable arm angle  $\psi$  to fulfil the primary task by following the trajectory and avoiding the limits of the joint as a secondary task.

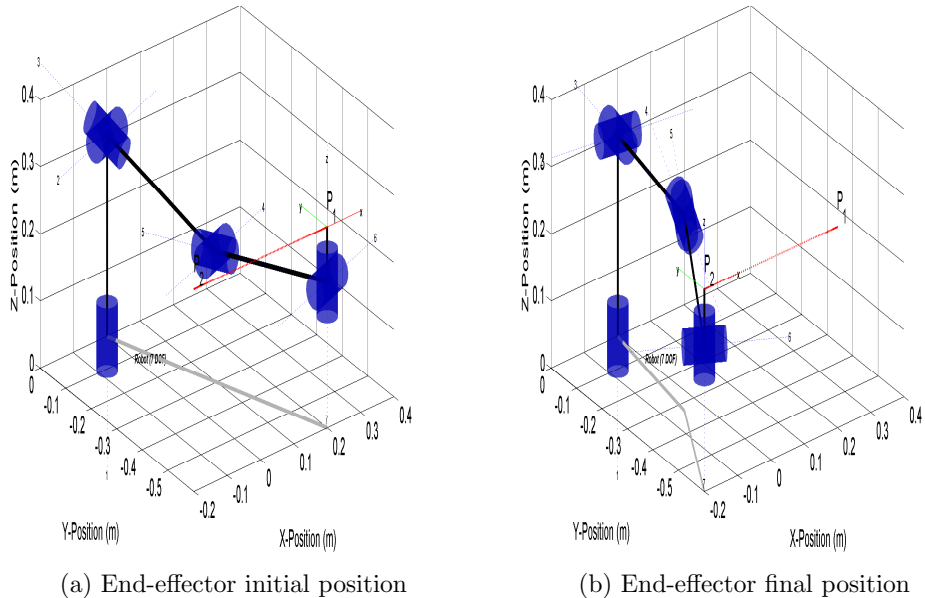


Figure 5-6: Straight line trajectory along X-axis.

Figure 5-6 shows the robot arm with planned trajectory along X-axis from the initial pose  $P_1$  to the final pose  $P_2$  where

$$P_1 = \begin{bmatrix} 1 & 0 & 0 & 0.2000 \\ 0 & 1 & 0 & -0.6000 \\ 0 & 0 & 1 & 0.3000 \\ 0 & 0 & 0 & 1.0000 \end{bmatrix} \quad \text{and} \quad P_2 = \begin{bmatrix} 1 & 0 & 0 & -0.2000 \\ 0 & 1 & 0 & -0.6000 \\ 0 & 0 & 1 & 0.3000 \\ 0 & 0 & 0 & 1.0000 \end{bmatrix}$$

The end-effector moved along the X-axis from 0.2 to -0.2 while the orientation of the tool is not changing. The Cartesian trajectory was generated using the Matlab command  $ctraj(P1, P2, t)$  which create homogeneous transform sequence from pose  $P_1$  to  $P_2$  with  $t$  time steps which selected to be 100. In the absence of any secondary requirements such joint limits, setting the redundant parameter to arbitrary predefined value would give a joint trajectory that leads the tool to follow the desired trajectory. However, in the presence of the joint limits, the redundancy need to be resolved at each intermediate point at the position level based on the method discussed in chapter 4. After removing the arm angle range that leads the joints to violate their limits, choosing any arm angle from the feasible arm angle range would give joint angles that correspond to the pose at the task space and these joint angles are in the permissible limits. The feasible arm angle range can be optimized more to perform other secondary tasks such as avoiding obstacle, reducing the elbow movements and others. Figure 5-7 shows the simulation results of the planned trajectory along x. The arm angle was selected from the first single interval from the allowable set of each pose on the path to be as the following

$$\psi = \frac{\psi_U - \psi_L}{3} + \psi_L \quad (5.4)$$

Where  $\psi_U$  is maximum allowable arm angle and  $\psi_L$  is the minimum allowable arm angle. The joint limits used in this example are as listed in table 5.1.

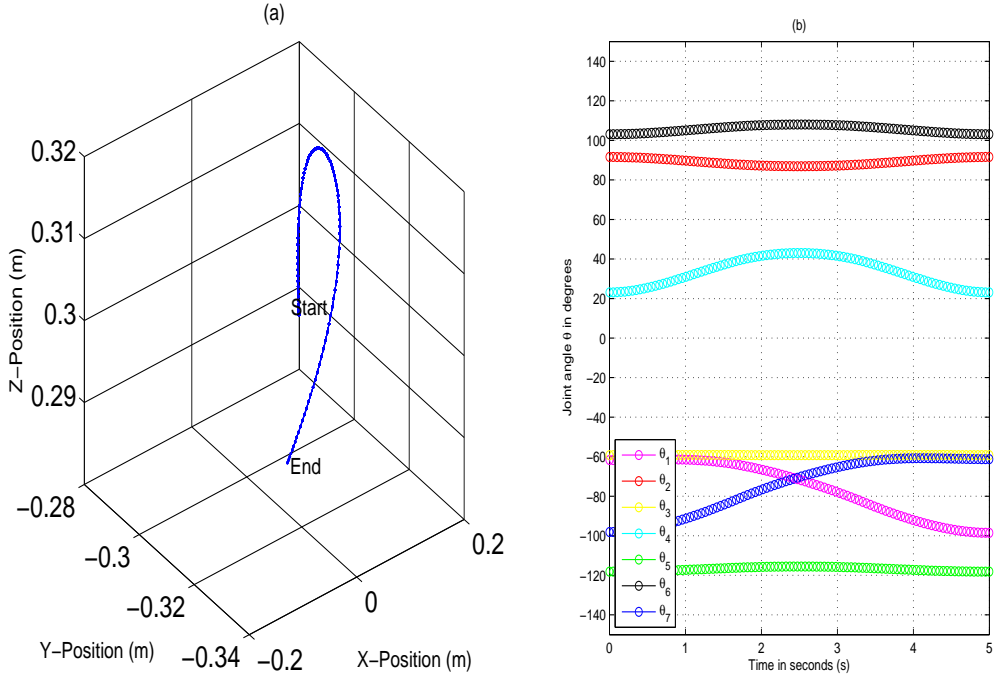


Figure 5-7: Simulation results of tracking straight line along X-axis when arm angle is as in (5.4) where (a): The elbow movement (b): The seven joint angle trajectories.

Figure (a) in 5-7 shows the elbow position path when the tool tracks the planned trajectory along X-axis and the arm angle is chosen to be as in (5.4). Figure (b) shows the corresponding computed joint trajectories. The results illustrates that the joints are inside the limits. This is one possible joint trajectory from many solutions that met the requirements of the joint limits. The forward kinematics discussed in chapter 3 is used to check the obtained results by using the acquired join angles to calculate the pose of the end-effector. The outcomes gained showed that the generated trajectory is exactly as the planned trajectory where the difference between the desired and generated trajectory is almost zero in ( $10^{-16}$ ), this emphasis how the analytical approach is accurate unlike an iterative method.

As mentioned before there are many joint trajectories in the redundant manipulators that can perform the same task at the Cartesian space. Let's choose another arm angle to be different from shown in (5.4) at each pose on the path that resolve the redundancy and computing the joint angles to follow the trajectory based on the method discussed before.

$$\psi = \psi_U - \frac{\psi_U - \psi_L}{3} \quad (5.5)$$

The results obtained using the arm angle described by (5.5) are shown in figure 5-8. The redundancy resolved to performed the tasks requirements by following the trajectory and avoiding the arm angles that exceed the limits of the joints. Figure (a) in 5-8 shows the elbow trajectory motion while tracking the planned straight line on the X-axis. The elbow trajectory is different from the elbow trajectory in figure 5-7 even though the same tasks are performed at the Cartesian space. Figure (b) in 5-8 shows the joint angle positions at the joint space. The results illustrates that these joint angle are inside the limits, some of these joint angle are different from the joint angles in figure 5-7 even thought the end-effector follows the same path.

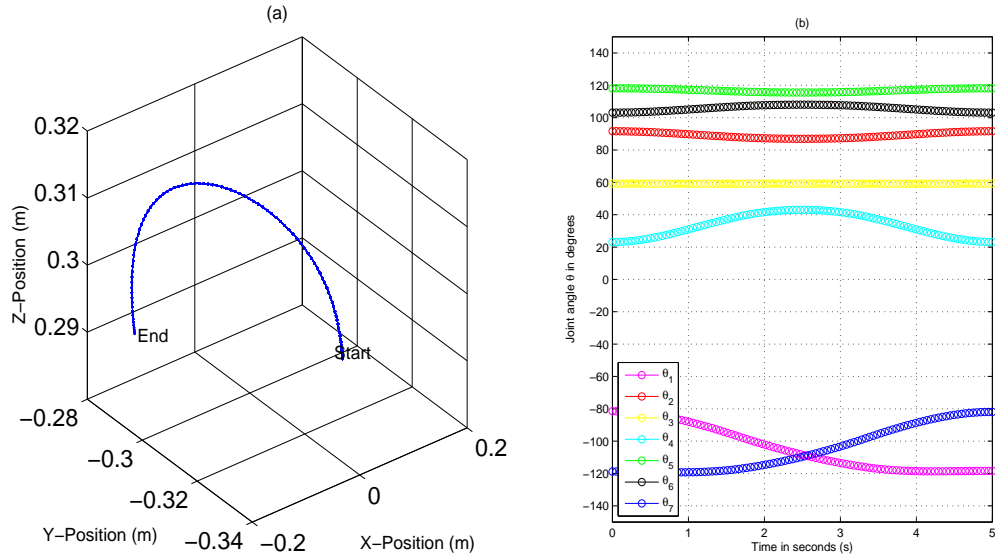


Figure 5-8: Simulation results of tracking straight line along X-axis when arm angle is as in (5.5) where (a): The elbow movement (b): The seven joint angle trajectories.

Another test was implemented on the Y-axis by moving the end-effector backward and forward. The trajectory generated in the same way as the path was created on X-axis. The initial pose  $P_1$  and the final pose  $P_2$  of the end-effector are as the following

$$P_1 = \begin{bmatrix} 1 & 0 & -0.0052 & -0.4000 \\ 0 & 1 & 0 & -0.2000 \\ 0.0052 & 0 & 1 & 0.5000 \\ 0 & 0 & 0 & 1.0000 \end{bmatrix} \quad P_2 = \begin{bmatrix} 1 & 0 & -0.0052 & -0.4000 \\ 0 & 1 & 0 & 0.2000 \\ 0.0052 & 0 & 1 & 0.5000 \\ 0 & 0 & 0 & 1.0000 \end{bmatrix}$$

Figure 5-9 illustrates the robot manipulator and the planned path on the Y-axis. The end-effector moved from -0.2 to 0.2 on the Y-axis while the X, Y coordinates and the orientation of the tool are not changing. At each pose on the path, the redundancy parameter was computed based on the joint limit constraints. Then the shoulder and wrist joint angles are acquired.

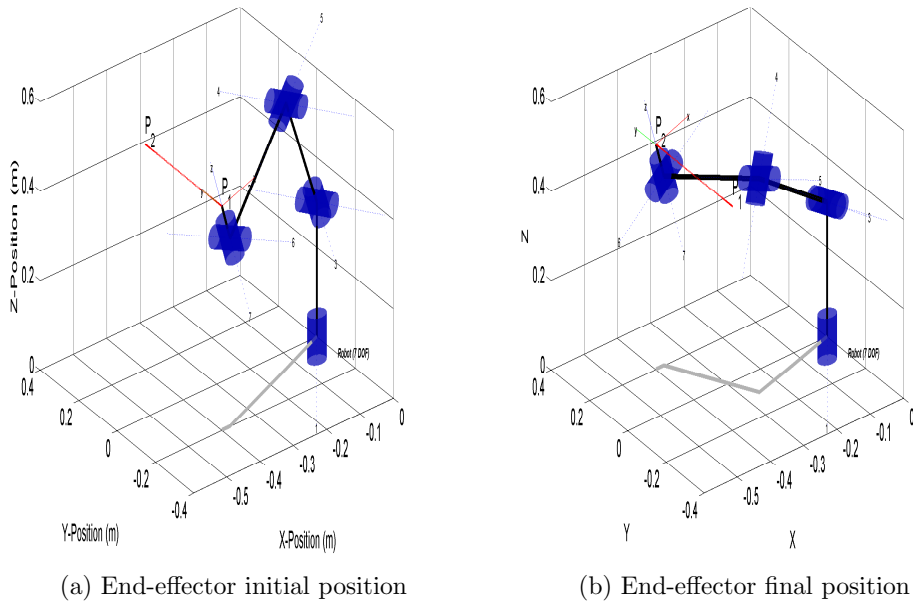


Figure 5-9: Straight line trajectory along Y-axis.

Based on the selected arm angle from the feasible arm angle range, the elbow movement and the joint trajectories were plotted. Different arm angles gives different joint trajectories. However, all the solutions are acceptable as long as the tool follow the path and the joint angles are inside the allowable range. Figure 5-10 shows one of the feasible solutions when the arm angle was chosen to be as in (5.4) between the maximum and minimum suitable arm angles at each pose on the path. Figure (a) in 5-10 shows the position path of the elbow while the end-effector tracking the path on the Y-axis. Figure b illustrates the joint trajectories that lead the tool to perform the task. The joint angles are inside the limits. These joint angles employed to calculate the pose of the tool, the results obtained were very accurate where the error between the generated and desired trajectory was almost zero in ( $10^{-16}$ ).

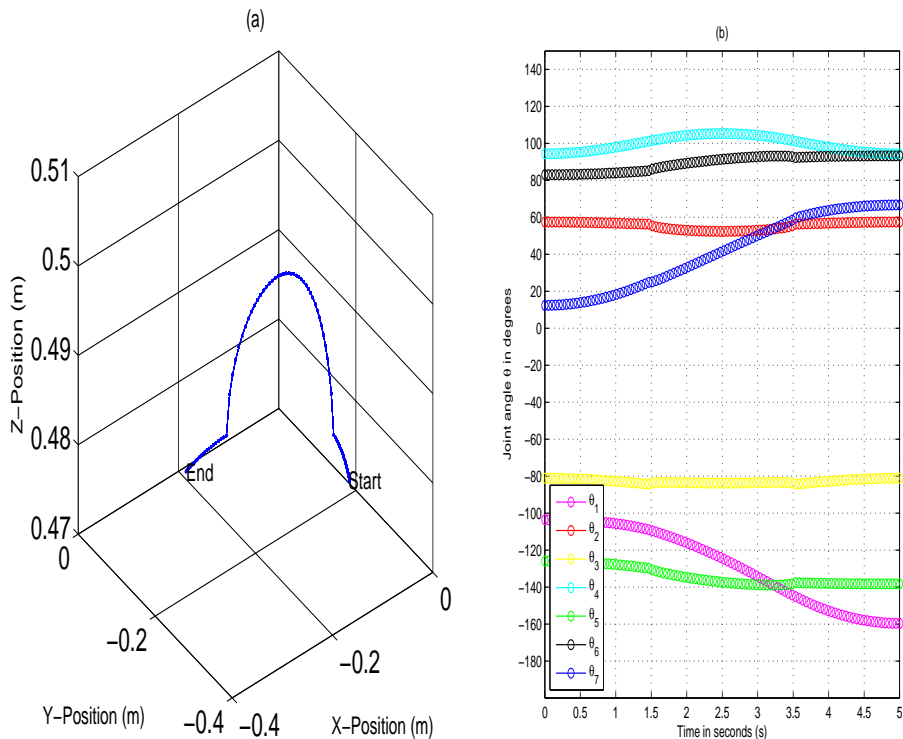


Figure 5-10: Simulation results of tracking straight line along Y-axis when arm angle is as in (5.4) where (a): The elbow movement (b): The seven joint angle trajectories.

Another arm angle was selected to be as in (5.5). A totally different elbow path was obtained as shown in figure 5-11 (a) with the same task at the Cartesian space. Some of the joint angle trajectories in figure 5-10 are totally different from the trajectories in figure 5-11. for example joint angle  $\theta_1$  moved from  $-100^\circ$  to  $-160^\circ$  in figure 5-10 while in figure 5-11 it went from  $160^\circ$  to  $100^\circ$ . The joint angle  $\theta_2$  and  $\theta_4$  are same in both figures. The joint angle  $\theta_5$  varies between  $-120^\circ$  and  $-140^\circ$  in figure 5-10 while it changed between  $140^\circ$  and  $120^\circ$  in figure 5-11. The joint angle  $\theta_3$  was almost constant at  $-80^\circ$  in figure 5-10 and at  $80^\circ$  in figure 5-11.

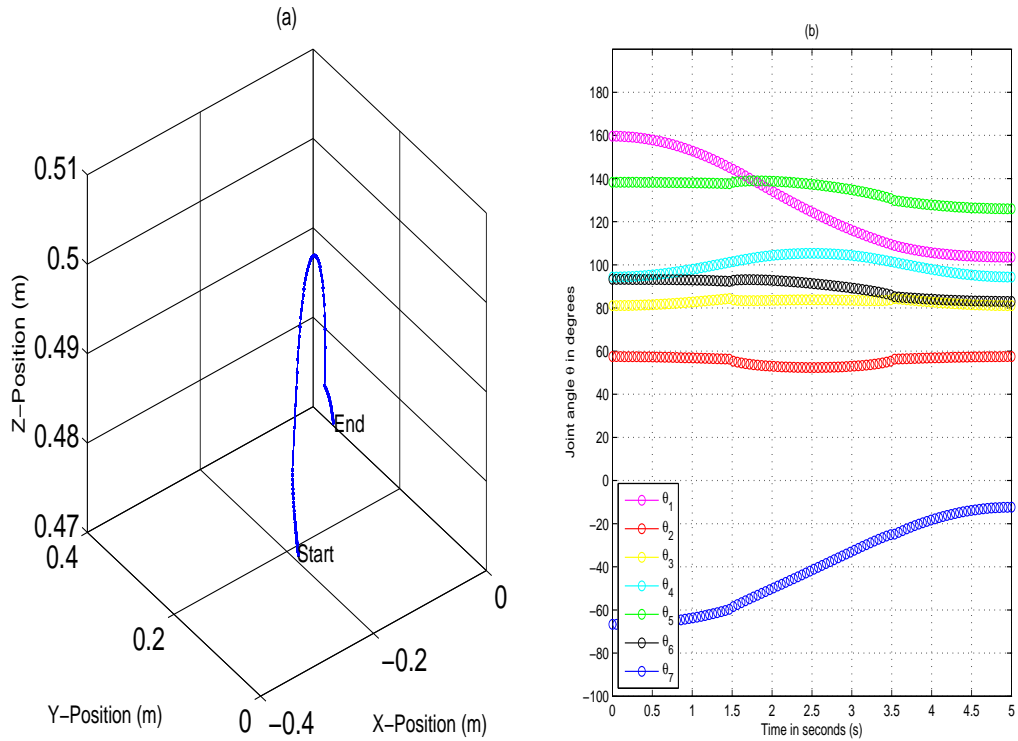


Figure 5-11: Simulation results of tracking straight line along Y-axis when arm angle is as in (5.5) where (a): The elbow movement (b): The seven joint angle trajectories.

The method was also tested on the Z-axis by moving the end-effector downward along the Z-axis while the X-Y coordinates and the orientation of the tool are not changing. The end-effector started at  $P_1$  and stop at  $P_2$  as the following

$$P_1 = \begin{bmatrix} 1 & 0 & -0.0052 & 0.5000 \\ 0 & -1 & 0 & 0.1000 \\ 0.0052 & 0 & -1 & 0.5000 \\ 0 & 0 & 0 & 1.0000 \end{bmatrix} \quad P_2 = \begin{bmatrix} 1 & 0 & -0.0052 & 0.5000 \\ 0 & -1 & 0 & 0.1000 \\ 0.0052 & 0 & -1 & 0 \\ 0 & 0 & 0 & 1.0000 \end{bmatrix}$$

Figure 5-12 shows the robot arm angle configuration using the robotics toolbox and the planned trajectory along the Z-axis. The end-effector planned to move from 0.5m to 0m downward. After applying the redundancy resolution at the position level we eliminate any arm angles that violate the joint limits. These solutions can be explored more to accomplish other requirements other than avoiding joint limits.

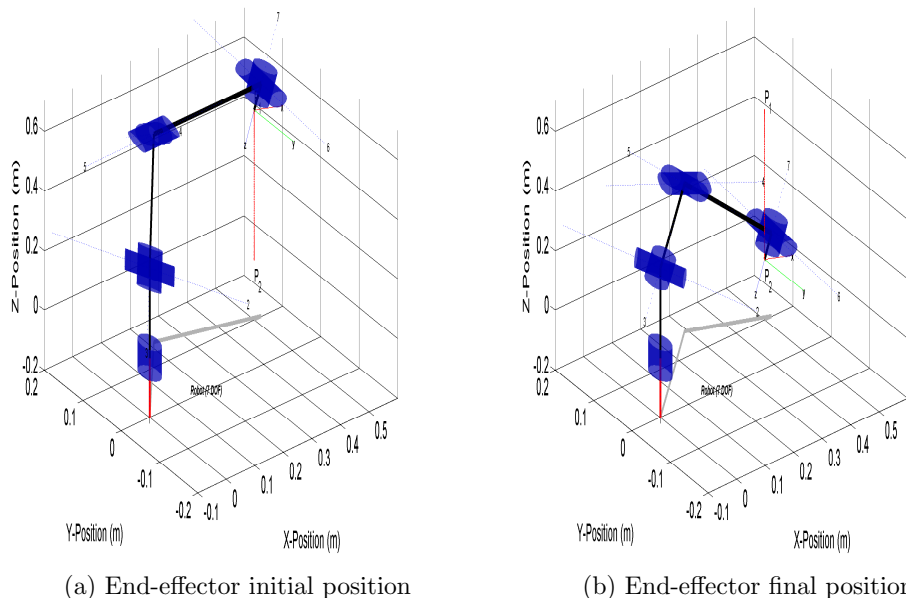


Figure 5-12: Straight line trajectory along Z-axis.

The redundancy resolution applied to follow the planned trajectory by choosing feasible arm angle then calculating the corresponding joint trajectories along Z-axis. In the following example, the maximum allowable arm angle was chosen to check the joint trajectories when  $\psi = \psi_U$ . This should make one of the joint angles to reach its maximum limits. Figure 5-13 (a) illustrates the elbow motion path and (b) shows the joint trajectory which illustrates that the joint angles  $\theta_3$  is reaching its maximum limits at  $180^\circ$ . This emphasizes that choosing any value greater than  $\psi_L$  would violate the limits of joint 3. The other joint angles are inside the admissible limits.

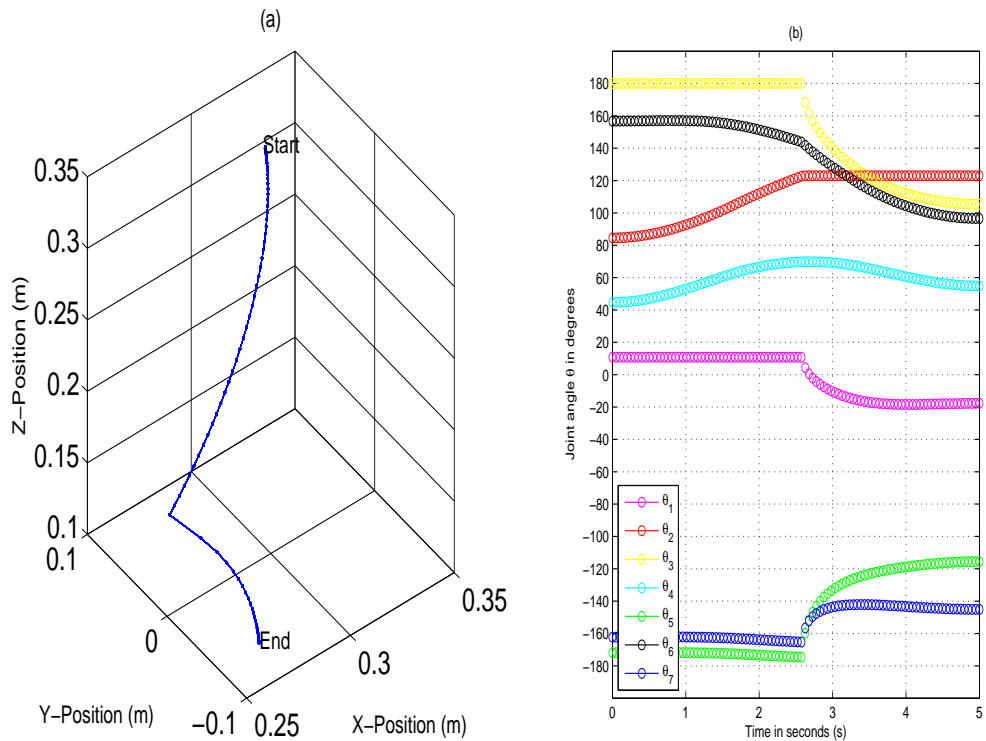


Figure 5-13: Simulation results of tracking straight line along Z-axis when arm angle is maximum where (a): The elbow movement (b): The seven joint angle trajectories.

Choosing the maximum arm angle as show in the previous example is not recommended because it lead some of the joint angles to reach their limits. This make semi-singularity in the manipulator, so its always better to stay far from the limits as much as possible. The redundancy parameter can be exploited more to avoid this kind of singularity. The following example shows the results obtained by choosing the arm angle at each pose on the trajectory to be as in (5.4). The results showing the all the joint are inside the limits of each joint.

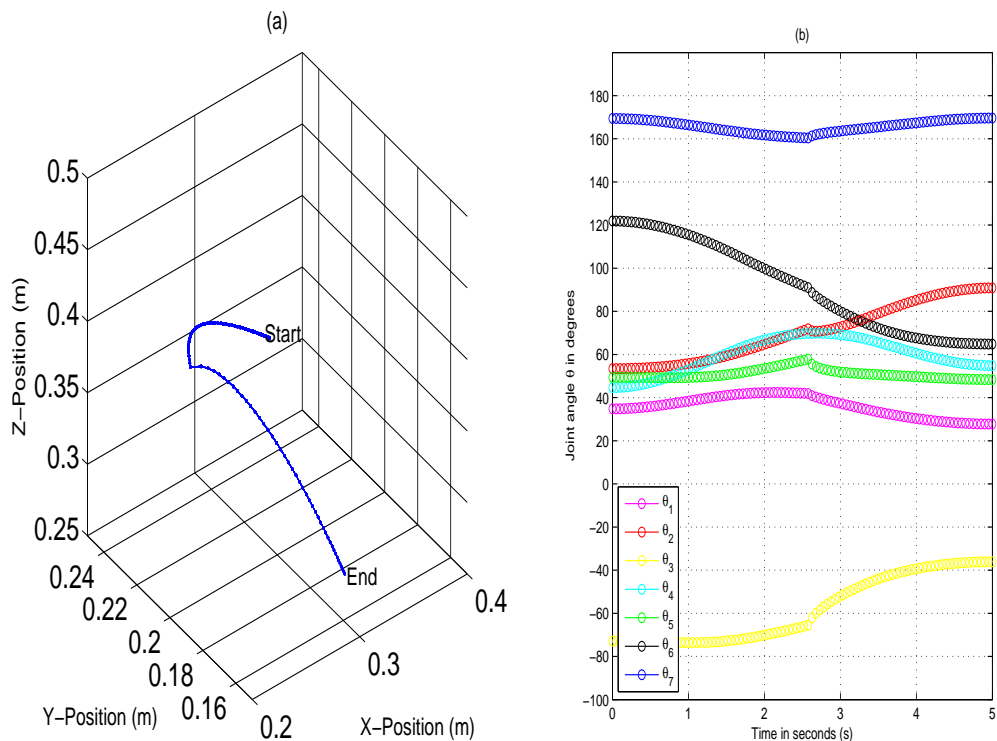


Figure 5-14: Simulation results of tracking straight line along Z-axis when arm angle is as in (5.4) where (a): The elbow movement (b): The seven joint angle trajectories.<sup>4</sup>



# Chapter 6

## Discussion and Conclusions

This chapter presents a general discussion section. Conclusions on the conducted work, and after that future work and ethical aspects are discussed.

### 6.1 Discussion

The forward kinematic equations and the corresponding algorithms for computation of the joint angles, derived in chapter 3 and 4, are tested and discussed in chapter 5. Firstly, the forward kinematics was used to plot the robot workspace and to check how the end-effector was accurate in tracking the planned trajectories. The self-motion of the arm, which appears in a form of a circle when the elbow rotating around the shoulder wrist axis, was defined in figure 4.1 and verified in section 5.3 with an example. The results showed how the joint limits were avoided successfully. The methods were implemented in Matlab and tested using Robotics toolbox.

Based on the outcomes obtained in the previous chapter, exploiting the redundancy in the 7-DOF manipulator at the position level rather than velocity level was a good choice. The method conducted in this project was not computationally expensive and it was very accurate. The use of the redundancy took place at the position level where no approximation was needed. With this method a direct control can be implemented for each joint. The problem of the work conducted is that the solutions

may become not continues in comparison with what can be achieved by solving the inverse kinematics at the velocity level. It also needs a full information about the trajectories in the task space not like exploiting the redundancy at the velocity level, which just requires to know the change of the end-effector velocity to compute the change of the joint velocities. I have spent time as well to extract XML Matlab files from the CAD model to have a better result validations but unfortunately that did not work. However, the results were verified using Matlab Robotics toolbox.

As mentioned in chapter 4, I followed the redundancy resolution methods to compute the joint angles proposed by [29]. This article was a great reference to this work because it is one of a few published papers that discussed the redundancy resolution for redundant manipulators with 7-DOF at the position level. The joint angles in this work have almost the same form as the joint angles in the article with some differences in the steps of computing the joints such as computing the reference joint angles of the shoulders. The article mentioned possibility for the redundancy exploitation to avoid the limits without showing the equations for computing the feasible arm angles for each pose. However, in this work all the equations and a step-by-step algorithm for keeping the angles within required ranges are presented and tested in simulations. Moreover, the redundancy methods explained in details for each joint angle.

I would say the objectives of the project were achieved. The literature review on the existing methods of solving the inverse kinematics for redundant manipulators with seven degree of freedom was conducted. Modeling the robot manipulator and deriving its forward kinematic equations were achieved. The inverse kinematic problem was solved by exploiting the redundancy at the position level. Scenarios to test the forward and inverse kinematics were also achieved.

According to the opponent's review on the report, the central theories and concepts of solving the inverse kinematics by exploiting the redundancy are clearly described. The objectives are met and have been clearly discussed in the report and the results are measured objectively and based facts.

I was interested in the beginning of this project to work also on the real robot set up once I finish my project primary requirements. However, regarding some personal issues even the work in the primary tasks was not conducted in continues time so there was a time delay in the project plan.

The most difficult part in this work was understanding how one can efficiently exploit the redundancy in the arm, which took most of the time. Making use of the redundancy to avoid the joint limits was as the main part of the work. The new thing in this work is that the equations for avoiding the joint limits at the position level for this kind of arm structure are derived and presented in this report. To the best of my knowledge, I have not seen work on such kind of robot arm that present the analytical methods to follow a trajectory at the positional level, which showed high accuracy and less computational cost.

Two arms similar to the LWA arm, considered in this work are used in the human-robot collaboration ABB YuMi [38], which is redundant and dexterous arm produced by ABB. The ABB YuMi is a dual-armed robot and each arm has seven revolute joints. According to ABB Robotics, this arm is so precise that it can thread a needle. This great level of precision make it perfect to perform complex tasks with small electronics materials. Other companies are manufacturing light weight arms such as the KUKA LBR iiwa which is a lightweight robot arm with 7 degrees of freedom [39] and the dual armed Motoman SDA series with 15 degrees of freedom [40].

The light weight arm studied in this thesis can play an important role in the upcoming forth industrial revolution [41] by making use of its redundancy intelligently with smart automation process. The current fast development of technology forms the basis of the forth industrial revolution. The use of internet in the cloud, robotics and artificial intelligence are also considered as drivers of the fourth industrial revolution [41], which is expected to lead to improving the quality of life and raising the global growth.

## 6.2 Conclusions

This thesis was devoted to model the 7-DOF articulated robot manipulator (LWA 10 kg payload by Schunk), to derive its forward kinematic equations and to solve the inverse kinematics by exploiting the redundancy in the manipulator. An extensive literature survey has been conducted on the existing methods of solving the inverse kinematics for redundant manipulators. Exploiting the redundancy on the position and velocity levels were studied. The forward kinematic equations were derived using the Denavit-Hartenberg convention. The redundancy was exploited at the position level to avoid the computational complexity and inaccuracy associated with exploiting the redundancy on the velocity level. The joint angles of the manipulator were computed in term of the redundancy parameter. The joint limit avoidance was addressed by choosing suitable redundancy parameter  $\psi$ . Then the singularity configurations were studied. The robot workspace was obtained using Monte Carlo methods, which is a random sampling method applied at the joint space. An example presented on how the self-motion of the arm appears when the end-effector is stationary. The methods applied to follow straight line trajectories while avoiding to exceed the limits of the joints. The results showed how solving the redundancy at the position level is being exact with low computational cost.

## 6.3 Future work

The redundancy parametrization on the position level discussed in this work opened the door for several future works. Beside exploiting the arm parameter to avoid the limits of the joint, it is possible to exploit the redundancy to meet other requirements. For example, the arm angle can be optimized to reduce the elbow movement by minimizing the distance between the current and the previous elbow positions. It can be used to avoid the obstacles as well. By knowing the obstacle position it is possible to calculate the correspondent arm angle that might lead the robot to crash with an obstacle by excluding this arm angle from the allowable arm angle range. It is also possible to study if this parametrization method can be applied to other robot manipulators with different structures.

## 6.4 Ethical aspects

In general, the applications of robotic arms are increasing everyday. Today, robots are in factories, hospitals and even in our houses. Due to this expanding, numerous ethical problems raised by engaging these robots in our daily life. Many factors need to be considered to avoid the robots misapply against the human. This research was conducted on a humanoid robot arm, which has exactly the same structure as the human arm. This robot arm can assist humans without arm because of its dexterity and flexibility that might be used in many circumstances and situations needed by the human [16]. However, the use of this kind of robot arm rise serious problems because unpredictable actions might hurt the human, for this reason several ethical aspects must be considered.

This robot is also used in the industries to perform various tasks such as pick and place, welding and assembling. Human interaction might be needed while performing these tasks, for this reason safety must be considered to avoid harming the workers. Fully automated industries where the human interaction is not required might solve the problem. However, this may increase the unemployment.



# Bibliography

- [1] Craig, J. J. (2005). *"Introduction to robotics: mechanics and control"*. Upper Saddle River: Pearson Prentice Hall.
- [2] Cheng, F. T., Chen, J. S., & Kung, F. C. (1998). *"Study and resolution of singularities for a 7-DOF redundant manipulator"*. Industrial Electronics, IEEE Transactions on, 45(3), 469-480.
- [3] Chan, T. F., & Dubey, R. V. (1995). *"A weighted least-norm solution based scheme for avoiding joint limits for redundant joint manipulators"*. Robotics and Automation, IEEE transactions on, 11(2), 286-292.
- [4] Shimizu, M., Kakuya, H., Yoon, W. K., Kitagaki, K., & Kosuge, K. (2008). *"Analytical inverse kinematic computation for 7-DOF redundant manipulators with joint limits and its application to redundancy resolution"*. Robotics, IEEE Transactions on, 24(5), 1131-1142.
- [5] Dubey, R. V., Euler, J., & Babcock, S. M. (1991). *"Real-time implementation of an optimization scheme for seven-degree-of-freedom redundant manipulators"*. Robotics and Automation, IEEE Transactions on, 7(5), 579-588.
- [6] Hollerbach, J. M. (1985, May). *"Optimum kinematic design for a seven degree of freedom manipulator"*. In Robotics research: The second international symposium (pp. 215-222). Cambridge, MIT Press.

- [7] Kreutz-Delgado, K., Long, M., & Seraji, H. (1992). “*Kinematic analysis of 7-DOF manipulators*”. The International journal of robotics research, 11(5), 469-481.
- [8] The arm virtual model (LWA4D) STL format <http://mobile.schunk-microsite.com>, [online March 2015].
- [9] G. K. Singh, J. Claassens, “*An analytical Solution for the Inverse Kinematics of a Redundant 7-dof Manipulator with Link Offsets*”, IEEE/RSJ Int. Conf. on Intelligent Robots and Systems (IROS), pp 2976-2982, 2010.
- [10] Siciliano, B. (1990). “*Kinematic control of redundant robot manipulators: A tutorial*”. Journal of Intelligent and Robotic Systems, 3(3), 201-212.
- [11] Seraji, H., Long, M., & Lee, T. (1991, April). “*Configuration control of 7 dof arms*”. In Robotics and Automation, 1991. Proceedings., 1991 IEEE International Conference on (pp. 1195-1200).
- [12] Colomé, A. (2011), “*Smooth Inverse Kinematics Algorithms for Serial Redundant Robots*”, (Doctoral dissertation, Institut de Robotica i Informatica Industrial (IRI), Universitat Politecnica de Catalunya (UPC), Barcelona, Spain).
- [13] Buss, S. R. (2004). “*Introduction to inverse kinematics with jacobian transpose, pseudoinverse and damped least squares methods*”. IEEE Journal of Robotics and Automation, 17(1-19), 16.
- [14] Lee, S., & Bejczy, A. K. (1991, April). “*Redundant arm kinematic control based on parameterization*”. In Robotics and Automation, 1991. Proceedings. IEEE International Conference on (pp. 458-465). IEEE.
- [15] Whitney, D. E. (1969). “*Resolved motion rate control of manipulators and human prostheses*”. IEEE Transactions on man-machine systems, Vol MMS-10(2), 47-53.
- [16] Siciliano, B., & Khatib, O. (Eds.). (2008), “*Springer handbook of robotics*”, Springer Science & Business Media.

- [17] Liegeois, A. (1977). “Automatic supervisory control of the configuration and behavior of multibody mechanisms”. IEEE transactions on systems, man, and cybernetics, 7(12), 868-871.
- [18] Fahimi, F. (2008). “Autonomous robots: modeling, path planning, and control”. Springer Science & Business Media.
- [19] Baillieul, J. (1986, April). “Avoiding obstacles and resolving kinematic redundancy”. In Robotics and Automation. Proceedings. 1986 IEEE International Conference on (Vol. 3, pp. 1698-1704).
- [20] Sciavicco, L., & Siciliano, B. (1988). “A solution algorithm to the inverse kinematic problem for redundant manipulators”. Robotics and Automation, IEEE Journal of, 4(4), 403-410.
- [21] Wampler, C. W. (1986). “Manipulator inverse kinematic solutions based on vector formulations and damped least-squares methods”. Systems, Man and Cybernetics, IEEE Transactions on, 16(1), 93-101.
- [22] Nakamura, Y., & Hanafusa, H. (1986). “Inverse kinematic solutions with singularity robustness for robot manipulator control”. Journal of dynamic systems, measurement, and control, 108(3), 163-171.
- [23] Klein, C. A., & Blaho, B. E. (1987). “Dexterity measures for the design and control of kinematically redundant manipulators”. The International Journal of Robotics Research, 6(2), 72-83.
- [24] Wang, J., Li, Y., & Zhao, X. (2010). “Inverse kinematics and control of a 7-dof redundant manipulator based on the closed-loop algorithm”. International Journal of Advanced Robotic Systems, 7(4), 1-9.
- [25] Seraji, H., & Colbaugh, R. (1990). “Improved configuration control for redundant robots”. Journal of Robotic Systems, 7(6), 897-928.

- [26] Asfour, T., & Dillmann, R. (2003). “*Human-like motion of a humanoid robot arm based on a closed-form solution of the inverse kinematics problem*”. In Intelligent Robots and Systems, 2003. Proceedings. 2003 IEEE/RSJ International Conference on (Vol. 2, pp. 1407-1412). IEEE.
- [27] Denavit, J. (1955). “*A kinematic notation for lower-pair mechanisms based on matrices*”. Trans. of the ASME. Journal of Applied Mechanics, 22, 215-221.
- [28] M.W. Spong, S. Hutchinson, M. WidyaSagar, “*Robot Modeling and Control*”, Wiley, 2006, [ISBN 0-13-123629-6].
- [29] Shimizu, M., Yoon, W. K., & Kitagaki, K. (2007). “*A practical redundancy resolution for 7 dof redundant manipulators with joint limits*”. In Robotics and Automation, 2007 IEEE International Conference on (pp. 4510-4516).
- [30] Seraji, H. (1989). “*Configuration control of redundant manipulators: Theory and implementation*”. Robotics and Automation, IEEE Transactions on, 5(4), 472-490.
- [31] Rodrigues’ rotation formula <https://en.wikipedia.org/wiki/Rodrigues> Accessed 02 Sep 2015.
- [32] Zhou, D., Ji, L., Zhang, Q., & Wei, X. (2015). “*Practical analytical inverse kinematic approach for 7-DOF space manipulators with joint and attitude limits*”. Intelligent Service Robotics, 8(4), 215-224.
- [33] Dahm, P., & Joublin, F. (1997). “*Closed form solution for the inverse kinematics of a redundant robot arm*”. Inst. Neuroinf, Ruhr-Univ. Bochum, 44780, 97-08.
- [34] Baillieul, J., Hollerbach, J. M., & Brockett, R. (1984). “*Programming and control of kinematically redundant manipulators*”. In IEEE. 1984.
- [35] Bedrossian, N. S. (1990). “*Classification of singular configurations for redundant manipulators*”. In Robotics and Automation, 1990. Proceedings., 1990 IEEE International Conference on (pp. 818-823).

- [36] Alciatore, D., & Ng, C. (1994). “*Determining manipulator workspace boundaries using the Monte Carlo method and least squares segmentation*”. ASME Robotics: Kinematics, Dynamics and Controls, 72, 141-146.
- [37] Luo, J., Wen, Q., He, J., & Ye, B. (2015). “*Workspace Analysis of 7-DOF Humanoid Robotic Arm*”. Manufacturing automation, 1, 2.
- [38] <http://www.robots.com/articles/viewing/human-robot-collaboration-with-the-abb-yumi>. Human robot collaboration with the ABB YuMi, [online Dec 2016].
- [39] The KUKA LBR iiwa is a lightweight robot arm with 7 degrees of freedom <http://www.babaimage.com/image/the-kuka-lbr-iiwa-is-a-lightweight-robot-arm-with-7-degrees-of-freedom>, [online Dec 2016].
- [40] Specifications of MOTOMAN Dual Arm Robots <http://www.dualarmrobot.com> specifications, [online Dec 2016].
- [41] Service robotics in the Fourth Industrial Revolution <http://ixion.es/service-robotics-in-the-fourth-industrial-revolution>, [online Nov 2016].





Shehab Mohammed  
Kinematic Motion Planning for a 7-Axis Robotic Arm (LWA70 by Schunk)  
Master Thesis in Electronic Engineering (Specialization Robotics and Control),  
5EL205, 30 hp